

# Cortical adaptation to sound reverberation

<sup>3</sup> Aleksandar Z Ivanov<sup>1</sup>, Andrew J King<sup>1</sup>, Ben DB Willmore<sup>1†</sup>, Kerry MM Walker<sup>1†</sup>,  
<sup>4</sup> Nicol S Harper<sup>1†</sup>

\*For correspondence:

aleksandar.ivanov@dpag.ox.ac.uk  
(FMS)

<sup>†</sup>These authors contributed  
equally to this work

<sup>5</sup> <sup>1</sup>Department of Physiology, Anatomy & Genetics, University of Oxford, United Kingdom

<sup>6</sup> 

---

<sup>7</sup> **Abstract** In almost every natural environment, sounds are reflected by nearby objects,  
<sup>8</sup> producing many delayed and distorted copies of the original sound, known as reverberation. Our  
<sup>9</sup> brains usually cope well with reverberation, allowing us to recognize sound sources regardless of  
<sup>10</sup> their environments. In contrast, reverberation can cause severe difficulties for speech recognition  
<sup>11</sup> algorithms and hearing-impaired people. The present study examines how the auditory system  
<sup>12</sup> copes with reverberation. We trained a linear model to recover a rich set of natural, anechoic  
<sup>13</sup> sounds from their simulated reverberant counterparts. The model neurons achieved this by  
<sup>14</sup> extending the inhibitory component of their receptive filters for more reverberant spaces, and  
<sup>15</sup> did so in a frequency-dependent manner. These predicted effects were observed in the  
<sup>16</sup> responses of auditory cortical neurons of ferrets in the same simulated reverberant  
<sup>17</sup> environments. Together, these results suggest that auditory cortical neurons adapt to  
<sup>18</sup> reverberation by adjusting their filtering properties in a manner consistent with dereverberation.

<sup>19</sup> 

---

## <sup>20</sup> Introduction

<sup>21</sup> Reverberations accompany almost all natural sounds that we encounter and are the reflections  
<sup>22</sup> of sound off objects in the environment such as walls, furniture, trees, and the ground (*Huisman*  
<sup>23</sup> and *Attenborough*, 1991; *Sakai et al.*, 1998). Compared to the original sound, these reflections  
<sup>24</sup> are attenuated and distorted due to frequency-selective absorption and delayed due to increased  
<sup>25</sup> path length (*Kuttruff*, 2017).

<sup>26</sup> Reverberation can be useful, helping us judge room size, sound-source distance, and realism  
<sup>27</sup> (*Shinn-Cunningham*, 2000; *Trivedi et al.*, 2009; *Kolarik et al.*, 2021). However, strong reverberation  
<sup>28</sup> can impair sound-source localization (*Hartmann*, 1982; *Shinn-Cunningham and Kawakyu*, 2003;  
<sup>29</sup> *Rakerd and Hartmann*, 2005; *Shinn-Cunningham et al.*, 2005) and segregation (*Culling et al.*, 1994;  
<sup>30</sup> *Darwin and Hukin*, 2000), pitch discrimination (*Sayles and Winter*, 2008) and speech recognition  
<sup>31</sup> (*Knudsen*, 1929; *Nábělek et al.*, 1989; *Guediche et al.*, 2014; *Houtgast and Steeneken*, 1985). Notably,  
<sup>32</sup> reverberation can be detrimental for people with hearing impairments, increasing tone de-  
<sup>33</sup> tection thresholds and reducing intelligibility of consonants (*Humes et al.*, 1986; *Heffner and Wilber*,  
<sup>34</sup> 1990). It can also impede the effectiveness of auditory prostheses such as hearing aids (*Schweitzer*,  
<sup>35</sup> 2003; *Qin and Oxenham*, 2005; *Poissant et al.*, 2006) and substantially reduces the performance of  
<sup>36</sup> automatic speech recognition devices (*Yoshioka et al.*, 2012; *Kinoshita et al.*, 2016).

<sup>37</sup> The auditory system has mechanisms to help us cope with reverberation, to the extent that  
<sup>38</sup> healthy listeners often only directly notice it when it is strong (in environments such as cathe-  
<sup>39</sup> drals). In the presence of mild-to-moderate reverberation, healthy listeners can continue to per-  
<sup>40</sup> form sound localization (*Hartmann*, 1982; *Rakerd and Hartmann*, 2005) and speech and auditory  
<sup>41</sup> object recognition tasks (*Houtgast and Steeneken*, 1985; *Bradley*, 1986; *Darwin and Hukin*, 2000;  
<sup>42</sup> *Culling et al.*, 2003; *Nielsen and Dau*, 2010). Since it is such a ubiquitous property of natural sounds,

43 these findings highlight the importance, for both normal and impaired hearing, of understanding  
44 how the brain copes with reverberation (*Xia et al., 2018*).

45 What are the neurophysiological mechanisms that support listening in reverberant environments?  
46 Previous studies have examined subcortical processes that facilitate localization of reverberant sounds (*Yin, 1994; Litovsky and Yin, 1998; Fitzpatrick et al., 1999; Spitzer et al., 2004; Tollin et al., 2004; Pecka et al., 2007; Devore et al., 2009; Kuwada et al., 2012; Kim et al., 2015; Brughera et al., 2020*), and how subcortical processing of synthetic periodic sounds is disrupted by reverberation (*Sayles and Winter, 2008*) and partially restored by compensatory mechanisms (*Slama and Delgutte, 2015*). Much less is known about the neural processing of speech and other complex natural sounds in the presence of reverberation. However, converging evidence from electrophysiological recordings in animals (*Rabinowitz et al., 2013; Moore et al., 2013; Mesgarani et al., 2014*) and from human EEG (*Khalighinejad et al., 2019*) and fMRI (*Kell and McDermott, 2019*) studies suggests that representations of sounds that are invariant to non-reverberant background noise emerge at the level of auditory cortex via neuronal adaptation to stimulus statistics (but see also *Lohse et al., 2020*). Auditory cortex may play a similar role in adaptation to reverberation. Indeed, speech and vocalization stimuli reconstructed from auditory cortical responses in awake ferrets more closely resemble their anechoic versions than the reverberant ones, even if the sounds were presented in reverberant environments (*Mesgarani et al., 2014*). Similar results have been found in humans using sound reconstructions from EEG measurements (*Fuglsang et al., 2017*). It remains unclear, however, whether the observed cortical invariance to reverberation can occur in the absence of top-down attention, and through what neural mechanisms this is achieved.

47 Here, we addressed these questions by using a model to predict what neural tuning properties  
48 would be useful for effective attenuation of reverberation (a normative “dereverberation model”).  
49 We then test these predictions using neural recordings in the auditory cortex of anesthetized ferrets.  
50 More specifically, we made reverberant versions of natural sounds in simulated rooms of  
51 different sizes. Next, we trained a linear model to retrieve the clean anechoic sounds from their re-  
52 verberant versions. Our trained model provided specific predictions for how the brain may achieve  
53 this task: with increased reverberation, neurons should adapt so that they are inhibited by sound  
54 energy further into the past, and this should occur in a sound frequency-dependent manner. We  
55 observed these predicted effects in the responses of auditory cortical neurons to natural sounds  
56 presented in simulated reverberant rooms, and show that they arise from an adaptive process.  
57 These results suggest that auditory cortical neurons may support hearing performance in reverber-  
58 ant spaces by temporally extending the inhibitory component of their spectrotemporal receptive  
59 fields.

## 77 **Results**

### 78 **Dereverberation model kernels show reverberation-dependent inhibitory fields**

79 We trained a dereverberation model to estimate the spectrotemporal structure of anechoic sounds  
80 from reverberant versions of those sounds. The anechoic sounds comprised a rich 10-minute-long  
81 set of anechoic recordings of natural sound sources, including speech, textures (e.g. running water)  
82 and other environmental sounds (e.g. footsteps) (see Sound stimuli and virtual acoustic space).  
83 Reverberation in small ( $3.0 \times 0.3 \times 0.3\text{m}$ ) and large ( $15 \times 1.5 \times 1.5\text{m}$ ) tunnel-shaped rooms was  
84 simulated using the virtual acoustic space simulator Roomsim (*Campbell et al., 2005*) (Figure 1A).  
85 The simulation also modelled the acoustic properties of the head and outer ear by using a ferret  
86 head-related transfer function (HRTF, *Schnupp et al., 2001*). The dimensions of the smaller room  
87 made it less reverberant (reverberation time,  $RT_{10} = 130\text{ms}$ ) than the larger room ( $RT_{10} = 430\text{ms}$ ).

88 After the reverberant sounds were generated, they were converted to cochleograms (Figure 1B).  
89 These spectrotemporal representations of the sound estimate the filtering and resulting represen-  
90 tation of the sound by the auditory nerve (*Brown and Cooke, 1994; Rahman et al., 2020*). Cochlea-  
91 grams of an example sound clip presented in the anechoic, small and large room conditions are

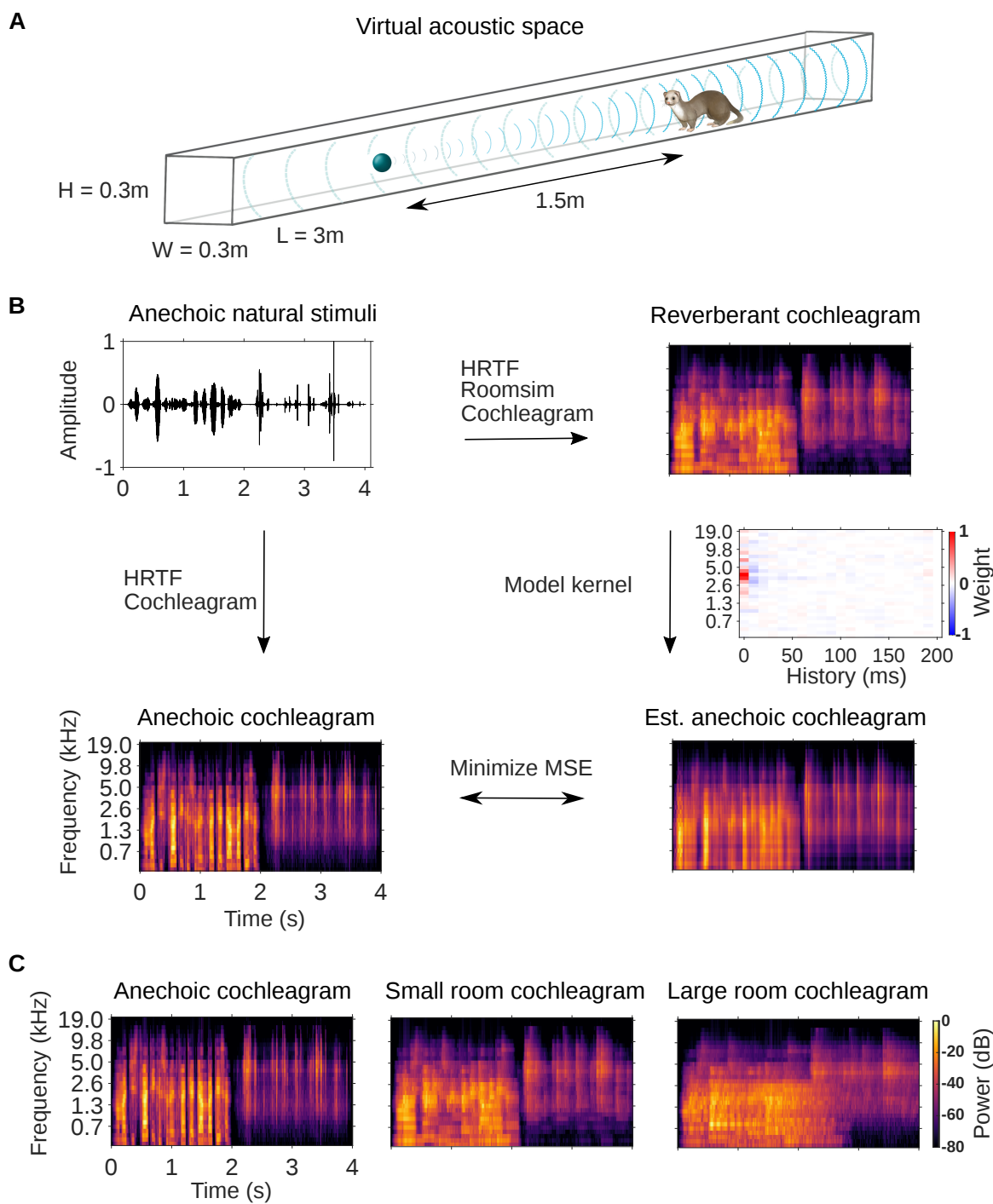


**Figure 1. Dereverberation model.**

**A**, Virtual acoustic space was used to simulate the sounds received by a ferret from a sound source in a reverberant room for diverse natural sounds. Schematic shows the simulated small room (length ( $L$ ) = 3m, width ( $W$ ) = 0.3m, height ( $H$ ) = 0.3m) used in this study, and the position of the virtual ferret's head and the sound source (1.5m from the ferret head) within the room. We also used a medium (x2.5 size) and large room (x5). The acoustic filtering by a ferret's head and ears was simulated by a head-related transfer function (HRTF). **B**, Schematic of the dereverberation model. The waveform (top left panel) shows a 4s clip of our anechoic recordings of natural sounds. For a given room, simulated room reverberation and ferret HRTF filtering were applied to the anechoic sound using Roomsim (Campbell *et al.*, 2005), and the resulting sound was then filtered using a model cochlea to produce a reverberant cochleagram (top right panel). A cochleagram of the anechoic sound was also produced (bottom left panel). For each room, a linear model was fitted to estimate the anechoic cochleagram from the reverberant cochleagram for diverse natural sounds. Each of the 30 kernels in the model was used to estimate one frequency band of the anechoic sound. One such model kernel is shown (middle right panel). Generating the estimated anechoic cochleagram (bottom right panel) involved convolving each model kernel with the reverberant cochleagram, and the mean squared error (MSE) between this estimate and the anechoic cochleagram was minimized with respect to the weights composing the kernels. **C**, Sample cochleograms of a 4s sound clip for the anechoic (left panel), small room (middle panel), and large room (right panel) reverberant conditions.

92 shown in Figure 1C.

93 We trained a dereverberation model to recover the anechoic cochleagram, using either the  
94 small or large room cochleograms as an input (Figure 1B). The dereverberation model was com-  
95 prised of a set of “dereverberation” kernels, one for each frequency in the anechoic cochleagram  
96 (see Model kernels). Each model kernel used the full reverberant cochleagram (up to 200ms in the  
97 past) to estimate the current power in the anechoic cochleagram within a single frequency band.  
98 This resulted in a set of positive and negative weights in each model kernel. Obtaining the esti-  
99 mated anechoic sounds involved convolution over time between the model kernels and the rever-  
100 berant cochleograms, and the model was trained to minimize the difference between this estimate  
101 and the original anechoic sound (Figure 1B). The model was trained separately to dereverberate  
102 the small and large room cochleograms. For each room, on a held-out test set, the dereverberation  
103 model reduced the difference between the incoming reverberant cochleagram and the anechoic  
104 cochleagram (small room mean squared error reduction 26%; large room reduction 20%).

105 Three examples of model kernels are shown in Figure 2A for the large room and the small  
106 room, with the anechoic frequency band they estimate indicated at the top. For each model ker-  
107 nel, the excitatory (red) and inhibitory (blue) weights represent spectrotemporal features in the  
108 reverberant cochleograms that are associated with increased or decreased power in the specified  
109 frequency band of the anechoic cochleagram, respectively. The majority of the excitatory and in-  
110 hibitory weights appear localized around a particular frequency, resembling the frequency tuning  
111 seen in auditory cortical neurons (*Bizley et al., 2005*). This is expected in our dereverberation  
112 model since each kernel aims to estimate the power in a given frequency band of the anechoic  
113 cochleagram.

114 The model kernels had temporally asymmetric structure, where strongest excitatory weights  
115 tended to occur first (Figure 2A), followed soon after by a longer inhibitory field. These excitatory  
116 and inhibitory timings are readily apparent when we plot the frequency-averaged positive and  
117 negative kernel weights (Figure 2B), and are a common feature across all kernels in the model (Fig-  
118 ure 2-Figure supplement 1A, and Figure 2-Figure supplement 2A). This pattern has been commonly  
119 observed in the spectrotemporal receptive fields (STRFs) of auditory cortical neurons (*deCharms*  
120 *et al., 1998; Linden et al., 2003; Harper et al., 2016; Rahman et al., 2019*), so our model qualitatively  
121 reproduces the basic frequency tuning and temporal characteristics of these auditory cortical neu-  
122 rons.

123 Importantly, we can compare the model kernels for the large room with those for small room.  
124 The inhibitory components of the large-room kernels tended to be delayed and longer in duration,  
125 relative to the small-room kernels (Figure 2B). In contrast, the temporal profile of the excitatory  
126 components was similar for the small and large rooms. We predicted that a comparable shift in  
127 inhibitory filtering could play a role in reverberation adaptation in auditory cortical neurons.

## 128 **Auditory cortical neurons have reverberation-dependent inhibitory fields**

129 To test the predictions of our dereverberation model *in vivo*, we presented to anesthetized ferrets  
130 an 80 sec subset of the natural sounds in the simulated small and large reverberant rooms (see  
131 Sound stimuli and virtual acoustic space). We did this while recording the spiking activity of neurons  
132 in the auditory cortex using Neuropixels high-density extracellular microelectrodes (*Jun et al., 2017*)  
133 (see Surgical procedure). Stimuli were presented as 40 sec blocks, in which all sounds were in the  
134 same reverberant room condition. This allowed neurons to adapt to the reverberation acoustics of  
135 the room. We recorded the responses of 2,244 auditory cortical units. Of these, the 696 units (160  
136 single units, 23%) which were responsive to the stimuli were used for further analysis (see Spike  
137 sorting).

138 We estimated the filtering properties of each unit by fitting a separate STRFs to the neuronal  
139 responses for each reverberant condition. Neuronal STRFs are linear kernels mapping the cochlea-  
140 gram of the sound stimulus to the time-varying firing rate of the neuron (*Theunissen et al., 2001*).  
141 The positive regions of an STRF represent sound features whose level is positively correlated with

142 the the neuron's spike rate, providing the "excitatory" part of the receptive field. Similarly, nega-  
143 tive regions of the STRF indicate features whose level is negatively correlated with the neural unit's  
144 spike rate, providing the "inhibitory" receptive field.

145 Examples of typical neuronal STRFs are shown in Figure 2C, and these can be compared to the  
146 model kernel properties of our dereverberation model above (Figure 2A). As mentioned above, the  
147 model kernels show some similarity to the STRFs typically reported for auditory cortical neurons  
148 (*deCharms et al., 1998; Linden et al., 2003; Harper et al., 2016; Rahman et al., 2019*). Likewise, the  
149 model kernels show similarity to the STRFs we present here, including having frequency tuning,  
150 early excitatory receptive fields and delayed inhibitory receptive fields (Figure 2D). These consis-  
151 tencies between the general features of our model and neurophysiological responses validated  
152 our use of this normative approach to capture neural response properties. We next examined if  
153 the model could predict neural adaptation to different reverberant conditions.

154 The important prediction we observed in the model was that the inhibitory fields tended to  
155 be more delayed and of longer duration in the large-room kernels versus the small-room kernels,  
156 whereas the excitatory field remained unchanged. Strikingly, we observed the same pattern in  
157 the neuronal STRFs in Figure 2D. This observation also held across different frequency channels in  
158 both the model and the data. (Figure 2-Figure supplement 1, Figure 2-Figure supplement 2).

### 159 **Similar effects of reverberation on the inhibitory fields of model kernels and audi- 160 tory cortical neurons**

161 Since both the dereverberation model and the neuronal STRFs had structure which varied accord-  
162 ing to the reverberation condition, we sought to investigate these effects quantitatively. We used  
163 two metrics to estimate the temporal dynamics of the inhibitory (and excitatory) components of  
164 the model kernels and neuronal STRFs: Center of mass (*COM*) and peak time (*PT*) (see Quantifi-  
165 cation of the temporal effects in model kernels and neuronal STRFs). The *COM* measured the  
166 average temporal delay of the inhibitory (*COM*<sup>-</sup>) or excitatory (*COM*<sup>+</sup>) components of the model  
167 kernels/neuronal STRFs (Figure 2B,D). The *PT* is the time at which the maximal inhibition (*PT*<sup>-</sup>) or  
168 excitation (*PT*<sup>+</sup>) occurred.

169 For each anechoic frequency channel in the dereverberation model, we calculated the differ-  
170 ence between the *COM*<sup>-</sup> for the kernels in the large room and small room conditions, providing 30  
171 *COM*<sup>-</sup> differences (1 for each channel), and did the same for the *COM*<sup>+</sup>. We plotted the distribution  
172 of these differences as histograms in Figure 3A. Similarly, a histogram of the *COM* difference be-  
173 tween the neuronal STRFs in the large and small room conditions is plotted for 696 cortical units in  
174 Figure 3B. We found that the *COM*<sup>+</sup> did not differ significantly between the small and large rooms,  
175 either for model kernels (median *COM*<sup>+</sup> difference = 0.97ms, Wilcoxon signed-rank test,  $p = 0.066$ )  
176 or neuronal STRFs (median *COM*<sup>+</sup> difference = 0.32ms,  $p = 0.39$ ). In contrast, the *COM*<sup>-</sup> showed  
177 clear dependence on room size. The inhibitory centers of mass were higher in the larger room  
178 for both the model kernels (median *COM*<sup>-</sup> difference = 7.9ms,  $p = 1.9 \times 10^{-6}$ ), and neuronal STRFs  
179 (median *COM*<sup>-</sup> difference = 9.3ms,  $p = 1.5 \times 10^{-66}$ ).

180 The results of our analysis of *PT* were largely consistent with our *COM* findings (Figure 3C,D).  
181 The peak time of the excitatory component (*PT*<sup>+</sup>) of model kernels did not differ between the small  
182 and large room (median *PT*<sup>+</sup> difference = 0.0ms,  $p = 1.0$ ), while *PT*<sup>+</sup> in the neural data showed a  
183 small but statistically significant increase in the large room (median *PT*<sup>+</sup> difference = 0.0ms,  $p =$   
184 0.014). The peak time of the inhibitory component, on the other hand, occurred much later in the  
185 large room, in both the model kernels (median *PT*<sup>-</sup> difference = 10ms,  $p = 3.7 \times 10^{-3}$ ) and neuronal  
186 STRFs (median *PT*<sup>-</sup> difference = 10ms,  $p = 1.5 \times 10^{-39}$ ). In general, there was more spread in the *COM*  
187 and *PT* in the neuronal data comparing to the dereverberation model. This is likely because, unlike  
188 in the model, which was focused purely on dereverberation, the auditory cortex subserves multiple  
189 functions and a diversity of STRF spans is useful for other purposes (e.g. prediction, *Singer et al., 2018*).  
190 Despite this, it is notable that the median *COM* and *PT* differences of the dereverberation  
191 model were of similar magnitude to those of the real data.

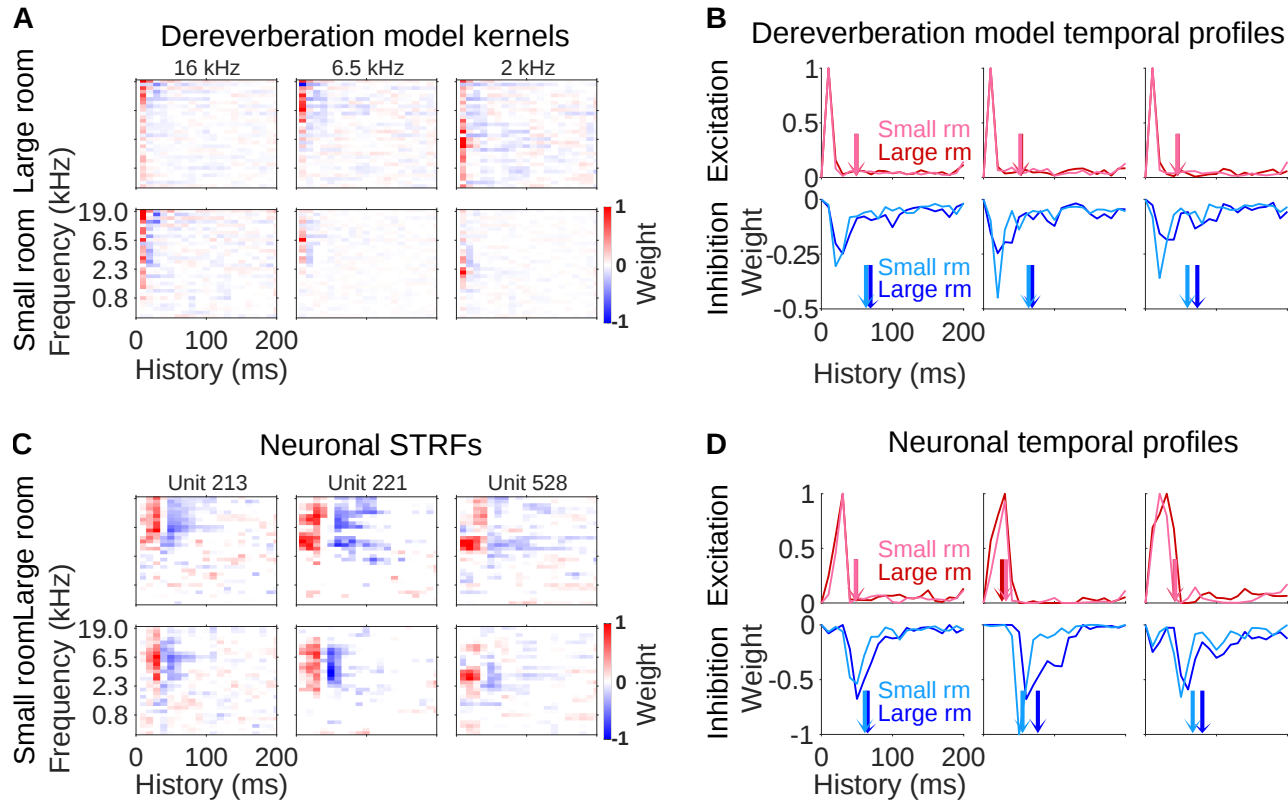


**Figure 2. Comparison of dereverberation model kernels and neuronal receptive fields from auditory cortex.**

**A**, Example model kernels resulting from the dereverberation model. Three example model kernels are shown, after training on the large (top row) or small (bottom row) room reverberation. The frequency channel which the model kernel is trained to estimate is indicated above each kernel. The color scale represents the weights for each frequency (y-axis) and time (x-axis). Red indicates positive weights (i.e. excitation), and blue indicates negative weights (i.e. inhibition; color bar right). **B**, Each plot in the top row shows the temporal profile of the excitatory kernel weights for the corresponding example model kernels shown in A. Excitatory temporal profiles were calculated by positively rectifying the kernel and averaging over frequency (the y-axis), and were calculated separately for the small (pink) and large (red) rooms. The center of mass of the excitation,  $COM^+$ , is indicated by the vertical arrows, which follow the same color scheme. The bottom row plots the inhibitory temporal profiles for the small (cyan) and large (blue) rooms. Inhibitory temporal profiles were calculated by negatively rectifying the kernel and averaging over frequency. The  $COM^-$  is indicated by the colored arrows. **C**, Spectrotemporal receptive fields (STRFs) of three example units recorded in ferret auditory cortex, measured for responses to natural sounds in the large room (top row) or small room (bottom row), plotted as for model kernels in A. **D** Temporal profiles of the STRFs for the three example units shown in C, plotted as for the model kernels in B.

**Figure 2-Figure supplement 1.** Model kernels and neuronal STRFs across frequency channels.

**Figure 2-Figure supplement 2.** Model and neuronal temporal profiles across frequency channels.

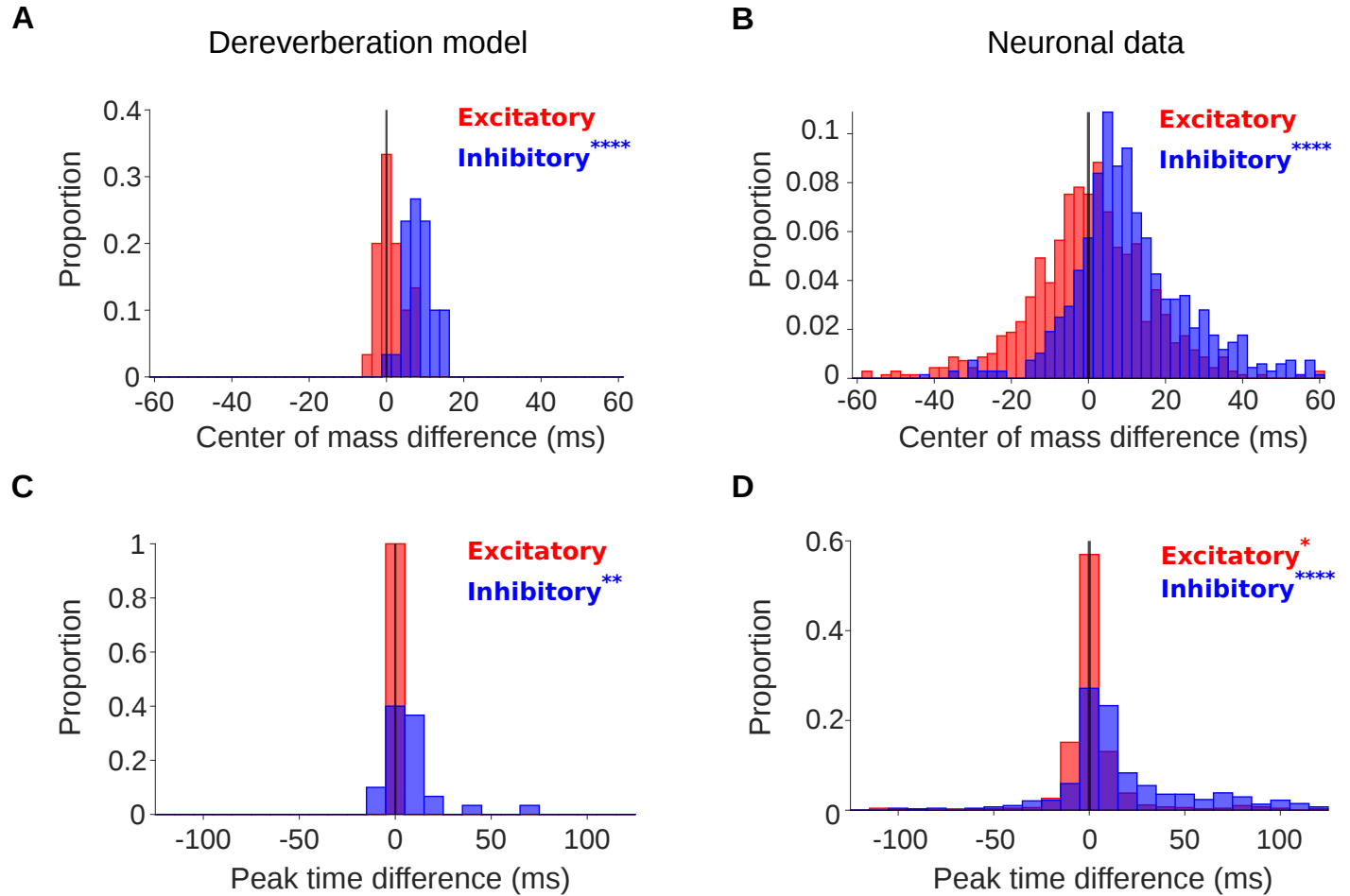


**Figure 3. Differences in the temporal profiles for large and small rooms.**

**A**, Histograms of the difference in center of mass of the temporal profiles (for the inhibitory field,  $COM^-$ , blue; excitatory field,  $COM^+$ , red) of dereverberation model kernels between the two different reverberant conditions (large - small room). The  $COM^-$  increased in the larger room with a median difference = 7.9ms;  $COM^+$  did not differ significantly between the rooms, median difference = 1.0ms. **B**, Center of mass differences, plotted as in A, but for the auditory cortical units. The  $COM^-$  increased in the larger room, median difference = 9.3ms;  $COM^+$  was not significantly different, median difference = 0.3ms. **C**, Histograms of the large - small room difference in peak time for the temporal profiles of the model kernels (inhibitory,  $PT^-$ , blue; excitatory,  $PT^+$ , red). The  $PT^-$  values were larger in the larger room, median difference = 10ms, whereas  $PT^+$  values were not significantly different, median difference = 0.0ms. **D**, Peak time differences for neuronal data, plotted as in C. The  $PT^-$  values increased in the larger room, median difference = 10ms, and  $PT^+$  showed a weakly significant change, but the median difference was 0ms. Asterisks indicate the significance of Wilcoxon signed-rank tests: \*\*\*\*  $p < 0.0001$ , \*\*  $p < 0.01$ , \*  $p < 0.05$ .

**Figure 3-Figure supplement 1.** A medium room condition shows intermediate center of mass and peak time values compared to the small and large room conditions.

**Figure 3-Figure supplement 2.** Simulated neurons suggest a role for adaptation in cortical dereverberation.

**Figure 3-Figure supplement 2.** Simulated neurons suggest a role for adaptation in cortical dereverberation (caption).

**Figure 3-Figure supplement 3.** Neural response to noise probe shows slower adaptation in the more reverberant condition.

**Figure 3-Figure supplement 4.** Adaptation to reverberation is confirmed using stimuli that switch between the small and large room.

192 As our stimulus set described above included only 2 reverberant rooms, it was not clear if the  
193 neurons treated these simulated rooms as two points along an ordered reverberation scale. To  
194 further examine whether the timing of the neuronal STRF inhibitory component scales with the  
195 amount of reverberation in our simulated room, we added a third “medium” sized room with the  
196 same relative proportions and absorption properties as the small and large rooms. We measured  
197 auditory cortical responses to this extended stimulus set in 2 ferrets (266 neural units).

198 The *COM* and *PT* measures of neuronal STRF dynamics were compared across the small,  
199 medium and large room conditions, and are shown in Figure 3-Figure supplement 1. As expected,  
200 there was little effect of room size on the timing of the excitatory STRF components (Figure 3-  
201 Figure supplement 1A,C). The *COM*<sup>+</sup> showed a weak but significant overall increase with room  
202 size (Kruskal-Wallis test;  $\chi^2(2) = 6.4$ ,  $p = 0.042$ ), but there was no effect of room size on the peak  
203 time of excitation, *PT*<sup>+</sup> ( $\chi^2(2) = 1.4$ ,  $p = 0.50$ ). In post-hoc pairwise comparisons, *COM*<sup>+</sup> only dif-  
204 fered between the small and medium rooms (Fisher’s least significant differences; large-small:  $p =$   
205 0.21; large-medium:  $p = 0.21$ ; medium-small:  $p = 0.012$ ).

206 In contrast, as predicted, we found that the delay of the inhibitory STRF components increased  
207 with greater room reverberation. The *COM*<sup>-</sup> was generally larger for larger rooms (Kruskal-Wallis  
208 test;  $\chi^2(2) = 37$ ,  $p = 7.6 \times 10^{-9}$ ) (Figure 3-Figure supplement 1B). Post-hoc pairwise tests confirmed  
209 that *COM*<sup>-</sup> differed between all three reverberant conditions (Fisher’s least significant differences;  
210 large-small:  $p = 1.3 \times 10^{-9}$ ; large-medium:  $p = 2.0 \times 10^{-4}$ ; medium-small:  $p = 0.019$ ). The peak time  
211 of STRF inhibition, *PT*<sup>-</sup>, also increased with room size across all 3 rooms ( $\chi^2(2) = 27$ ,  $p = 1.6 \times 10^{-6}$ ;  
212 large-small:  $p = 2.7 \times 10^{-7}$ ; large-medium:  $p = 0.0024$ ; medium-small:  $p = 0.036$ ) (Figure 3-Figure  
213 supplement 1D).

214 Thus, as room size, and hence reverberation time, was increased, we observed an increase  
215 in the delay of inhibition in the tuning properties of auditory cortical neurons. This increase is  
216 consistent with a normative model of dereverberation, suggesting that the tuning properties of  
217 auditory cortical neurons may adapt in order to dereverberate incoming sounds.

### 218 **Reverberation effects result from an adaptive neural process**

219 In principle, there could be other reasons, unrelated to adaptation, why the temporal profile of  
220 the inhibitory field is delayed and broader in the more reverberant room. An important possibility  
221 is that differences in sound statistics between the reverberation conditions could result in differ-  
222 ent STRFs, even if the underlying neuronal tuning is unchanged. For example, the cochleograms  
223 of more reverberant sounds are more temporally blurred (Figure 1C). This could lead to slower  
224 features in the neuronal STRFs for the larger room, purely due to systematic model fitting arte-  
225 facts (*Christianson et al., 2008*). In combination with changing sound statistics, a non-adaptive  
226 static non-linearity in the neural system could produce apparent differences in neuronal tuning  
227 between the reverberation conditions (*Christianson et al., 2008*). Here, we perform several addi-  
228 tional experiments and analyses to test whether the reverberation-dependent effects observed  
229 above are likely to result from a genuine adaptive process.

230 As a first test, for each recorded unit, we fitted a simulated linear-nonlinear-Poisson model  
231 neuron (*Schwartz et al., 2006*), composed of a single STRF (fitted to the combined small and large  
232 room stimuli) feeding into a non-linear output function (see subsection Simulated neuron), which,  
233 in turn, fed into a non-homogeneous Poisson process. Since this model did not have an adaptive  
234 component, we used it to assess whether our reverberation-dependent results could arise from fit-  
235 ting artefacts in a non-adaptive neuron. To do this, we presented the same stimuli to the simulated  
236 non-adaptive neurons as we did to the real neural responses and performed the same analyses.  
237 Hence, we fitted STRFs to the simulated neural responses separately for the large and small room  
238 conditions. We then extracted *COM* and *PT* parameters from the excitatory and inhibitory tem-  
239 poral profiles of these STRFs, and compared them to those of the measured cortical units. The  
240 simulated results are shown alongside the neural results in Figure 3-Figure supplement 2.

241 We asked whether the shift in inhibition observed in the dereverberation model and neural

242 data was also present in this adaptation-free simulation. In the simulation, although the inhibitory  
243  $COM^-$  was slightly larger for the more reverberant condition (Figure 3-Figure supplement 2B), the  
244 effect size for the simulated neurons (median  $COM^-$  difference = 0.90ms,  $p = 1.5 \times 10^{-5}$ ) was very  
245 small compared to that observed in the real neuronal data (median  $COM^-$  difference = 9.3ms,  $p =$   
246  $1.5 \times 10^{-66}$ , Figure 3-Figure supplement 2C). We directly compared the  $COM^-$  room differences be-  
247 tween cortical units and their simulated counterparts (Figure 3-Figure supplement 2D), and found  
248 that the reverberation effects on  $COM^-$  were consistently larger in the neuronal data (median  
249 difference = 9.3ms,  $p = 3.9 \times 10^{-35}$ ). An analysis of the peak time of inhibitory STRF components  
250 for neural and simulated units was in agreement with the center of mass results (Figure 3-Figure  
251 supplement 2E-G). The simulation predicted a near zero shift in the peak inhibitory component be-  
252 tween rooms (median  $PT^-$  difference = 0ms,  $p = 3.5 \times 10^{-9}$ ), and was unable to account for the 10ms  
253 large room delay observed in the neuronal responses (median difference = 10ms,  $p = 4.7 \times 10^{-31}$ ). For  
254 the simulation, differences in  $COM^+$  and  $PT^+$  between the two reverberation conditions were small  
255 (Figure 3-Figure supplement 2B,E, median  $COM^+$  difference = 1.7ms,  $p = 3.4 \times 10^{-4}$ ; median  $PT^+$  dif-  
256 ference = 0.0ms,  $p = 2.3 \times 10^{-30}$ ), with a slight difference from the real responses for  $PT^+$  difference  
257 (median difference = 0.0ms,  $p = 7.7 \times 10^{-6}$ ) but not  $COM^+$  difference (median difference = 0.0ms,  $p =$   
258 = 0.72). In summary, differences in stimulus properties alone were not able to account for the  
259 ~10ms delay in inhibitory  $COM$  timing in the large reverberant room, and these are likely to arise  
260 instead from neural adaptation to room reverberation.

261 To further confirm that the shift in inhibitory receptive fields arises from neuronal adaptation  
262 to reverberation and not to differences in stimulus statistics between the room conditions, we  
263 compared how all neurons in our dataset respond to a probe stimulus (a non-reverberated noise  
264 burst) interspersed within the small and large room reverberation stimuli (see Noise burst analy-  
265 sis). If the neurons adapt to the current reverberation condition, we should expect them to respond  
266 differently to the noise probe when it occurs within the small room and large room stimuli, reflect-  
267 ing the different adaptation states of the neurons. The neuronal responses to the noise probe  
268 showed a similar initial onset excitation (0-20ms) in both conditions, but the return to baseline  
269 firing was slower in the large room condition (Figure 3-Figure supplement 3A). This is consistent  
270 with the previous STRF analysis, wherein the excitatory temporal profile was similar between the  
271 small and large rooms (Figure 3B,D), while the inhibitory components were delayed in time in the  
272 large room (Figure 3B,D). For each cortical unit, we compared the center of mass of the noise burst  
273 response between the small and large rooms (Figure 3-Figure supplement 3B). The  $COM$  of the  
274 noise response increased slightly in the large room (median  $COM$  difference = 1.0ms,  $p = 0.0063$ ).  
275 Therefore, responses to an anechoic probe noise show further evidence for reverberation adap-  
276 tation in auditory cortical neurons, and are consistent with the predicted delayed inhibition in the  
277 presence of increased reverberation.

278 To further confirm and explore the adaptive basis of our results, we presented our reverberant  
279 sounds in blocks, which switched between the small and large room every 8s (see Figure 3-Figure  
280 supplement 4A and Switching stimuli analysis). This switching stimulus was tested in 310 neurons  
281 across 4 ferrets. If the room adaptation accumulates throughout the 8s following a room switch, we  
282 would expect the inhibitory component of neuronal STRFs to be increasingly delayed throughout  
283 this period. To test this prediction, we fitted STRFs to neuronal responses separately from the first  
284 and last half of each 8s room block, for the small (S1 early and S2 late halves) and large room (L1  
285 early and L2 late halves). The switching stimulus was designed to ensure that the stimulus set of  
286 L1 and L2 (or S1 and S2) was the same, but the order of stimuli was shuffled differently for these  
287 two time periods. Specifically, we predicted that the neuronal STRFs would have a larger  $COM^-$   
288 during the L2 than the L1 period, while  $COM^+$  should remain unchanged. By the same reasoning,  
289 in a large-to-small room switch, we expected the  $COM^-$  to be smaller in S2 than in S1, while  $COM^+$   
290 should remain similar.

291 We observed these predicted trends in our data, as shown in Figure 3-Figure supplement 4B,C.  
292 The  $COM^-$  decreased from S1 to S2 (median difference = -0.9ms, Wilcoxon signed-rank test,  $p =$

293 0.019), while  $COM^+$  did not change across these two periods (median difference = 0.52ms, p =  
294 0.85). In the switch to a large room,  $COM^-$  increased from the first (L1) to second (L2) half of the  
295 block (median difference = 1.5ms, p = 0.0088), while  $COM^+$  did not change (median difference =  
296 0.8ms, p = 0.35). These results further suggest that auditory cortical receptive fields are genuinely  
297 adapting dynamically to the changing reverberant conditions.

### 298 **Frequency dependence of the temporal profile of adaptation**

299 Reverberation is a frequency-dependent effect, as higher frequencies are usually attenuated by air  
300 and surfaces faster than lower ones in natural conditions (*Traer and McDermott, 2016; Kuttruff,*  
301 *2017*). Therefore, we explored whether our dereverberation model and auditory cortical neurons  
302 also show frequency-dependent reverberation effects.

303 Figures 2-Figure supplement 1 and Figure 2-Figure supplement 2 plot the reverberation model  
304 kernels and neuronal STRFs as a function of their frequency tuning. A visual inspection of these  
305 plots reveals that in both the model and the neuronal data, while the temporal spread of the ex-  
306 citatory components stays relatively constant across the preferred frequency, the inhibitory com-  
307 ponents tend to extend less far back in time as the preferred frequency increases. This tempo-  
308 ral narrowing of the inhibitory fields is observed for both the large and the small reverberant  
309 rooms. Therefore, the frequency-dependent effects predicted by our dereverberation model are  
310 confirmed in our cortical recordings.

311 To further examine these frequency-tuning effects, we plotted the excitatory and inhibitory  
312 center of mass values ( $COM^+$ ,  $COM^-$ ) as a function of the anechoic frequency estimated by the  
313 model kernels (Figure 4A) or the best frequency of the neuronal STRFs, i.e. the sound frequency of  
314 the highest weight (Figure 4B). The inhibitory components occurred systematically later in model  
315 kernels that were tuned to lower frequencies, in both the small (Pearson's correlation:  $r = -0.57$ ,  $p$   
316 = 0.0037) and large room ( $r = -0.80$ ,  $p = 2.6 \times 10^{-6}$ ) simulations. The same correlation between best  
317 frequency and  $COM^-$  was present in the neuronal STRFs (small room:  $r = -0.80$ ,  $p = 3.0 \times 10^{-6}$ ; large  
318 room:  $r = -0.85$ ,  $p = 1.6 \times 10^{-7}$ ). In contrast, the dereverberation model showed a smaller magnitude  
319 but significant increase of the excitatory  $COM^+$  with best frequency (small room:  $r = 0.52$ ,  $p$   
320 = 0.0087; large room:  $r = 0.55$ ,  $p = 0.0049$ ), while there was no relationship between  $COM^+$  and best  
321 frequency in the neuronal data (small room:  $r = -0.34$ ,  $p = 0.1$ ; large room:  $r = -0.25$ ,  $p = 0.24$ ).

322 Figure 4A,B also show that the inhibitory components were later in time in the large room than  
323 in the small room across the entire best frequency range, for both the dereverberation model and  
324 neuronal data. The  $COM^+$  values, on the other hand, were largely overlapping between the two  
325 rooms across this frequency range. This is in agreement with our observations that the inhibitory  
326 components of the receptive fields shift reliably with room size, while the excitatory components  
327 do not.

328 The frequency dependence of the inhibitory shift may reflect a frequency dependence in the  
329 reverberation acoustics themselves. The decay rate of the power in the impulse response of a  
330 reverberant environment depends on sound frequency, and this dependence can change across  
331 different environments. However, many man-made and natural environments show a gradual  
332 decrease in decay rate above about  $\sim 0.5$ kHz (*Traer and McDermott, 2016*). The early decay rate  
333 can be measured as the reverberation time  $RT_{10}$ , which is the time necessary for the sound level to  
334 decay by 10dB relative to an initial sound impulse. The frequency-dependent  $RT_{10}$  values for our  
335 small and large rooms are plotted in Figure 4C. The impulse responses of both rooms exhibited a  
336 decrease in  $RT_{10}$  values as a function of frequency (Pearson's correlation; small room:  $r = -0.82$ ,  $p$   
337 =  $1.1 \times 10^{-10}$ ; large room: Pearson's correlation:  $r = -0.91$ ,  $p = 8.0 \times 10^{-10}$ ). Therefore, the frequency-  
338 dependent delay in the inhibitory components of our dereverberation model and cortical STRFs  
339 paralleled the  $RT_{10}$  frequency profile of the virtual rooms in which the sounds were presented.

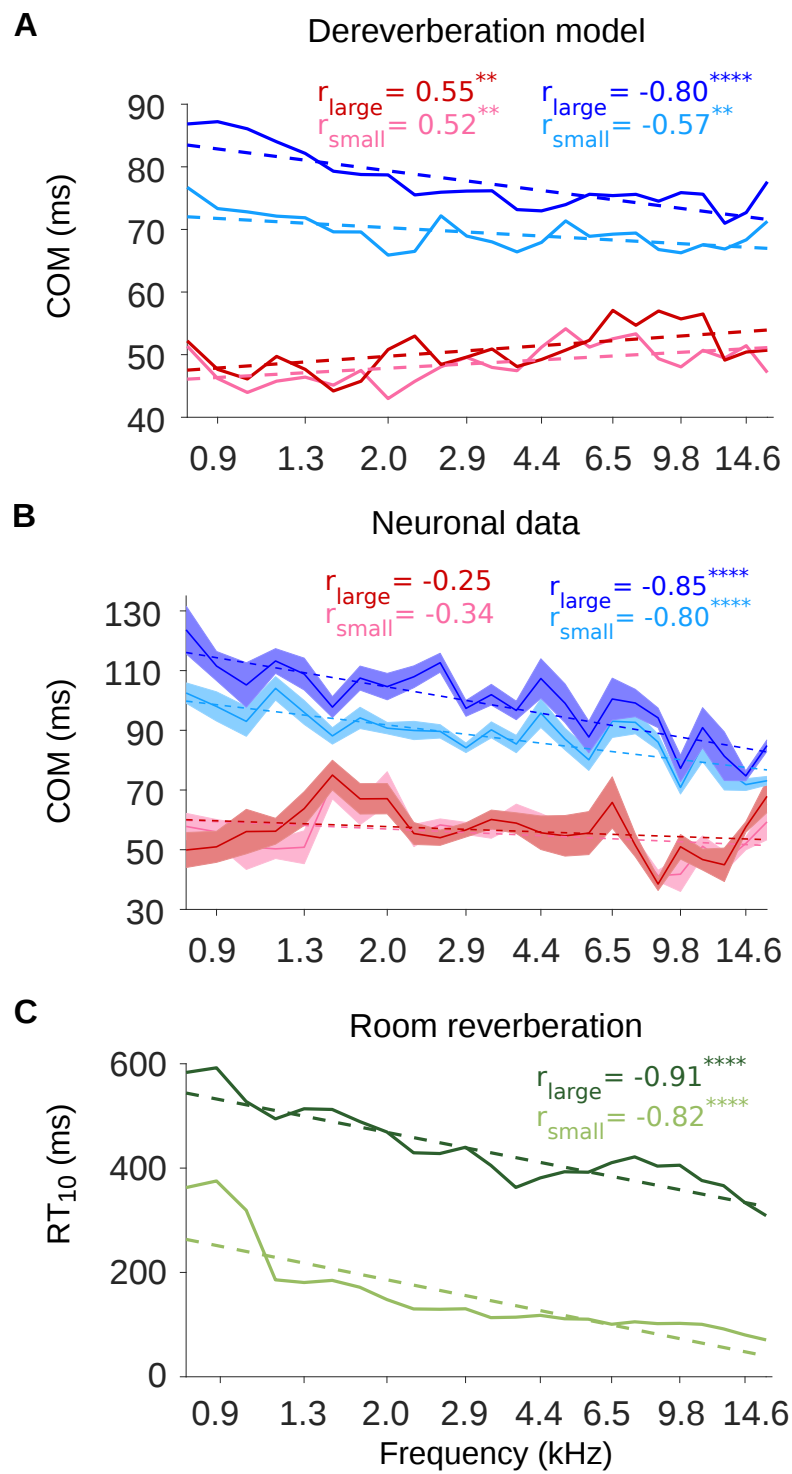


**Figure 4. The inhibitory field latencies are frequency dependent, consistent with the reverberation.**

**A**, Center of mass values (COM) are plotted against the anechoic frequency channel being estimated, for the excitatory and inhibitory fields of each model kernel for the large room and for the small room. These are color coded as follows: excitatory COM (large room,  $COM_{large}^+$ , red; small room,  $COM_{small}^+$ , pink) and their inhibitory counterparts ( $COM_{large}^-$ , blue;  $COM_{small}^-$ , cyan). The dashed lines show a linear regression fit for each room, and the Pearson's r value for each fit is given in the top right corner of the plot. **B**, COM values are plotted against the best frequency for the neuronal data (sound frequency of highest STRF weight). Each neuron was assigned a best frequency and the COM values measured. The solid lines represent the mean COM value for each best frequency, the shaded areas show  $\pm$  SEM; color scheme and other aspects as in A. **C**,  $RT_{10}$  values are plotted as a function of cochlear frequency bands, for the large (dark green) and small (light green) rooms. Linear regression fit (dotted line) was used as in A and B to calculate r. Significance of Pearson's correlation: \*\*\*\* $p < 0.0001$ , \*\* $p < 0.01$ .

## 340 Discussion

341 In this study, we applied a normative modelling approach to ask the question: If a function of the  
342 auditory system is to remove reverberation from natural sounds, how might the filtering prop-  
343 erties of neurons adapt to achieve this goal? To answer this question we used a rich dataset of  
344 anechoic speech and natural environmental sounds, adding different amounts of reverberation  
345 to them. We then trained a linear dereverberation model to remove this reverberation. We con-  
346 structed our model in such a way that the selectivity (kernels) of the model units after training can  
347 be compared to the filtering properties (STRFs) of real auditory cortex neurons in the ferret (Fig-  
348 ure 1). We confirmed the validity of our dereverberation model by showing that it recapitulated  
349 known properties of auditory cortical neurons, such as frequency tuning and temporally asymmet-  
350 ric STRFs with excitation followed by inhibition (Figure 2). Interestingly, our dereverberation model  
351 also makes two novel predictions: (1) the inhibitory components of neuronal STRFs should be more  
352 delayed in more reverberant conditions (Figure 3); and (2) the inhibition should occur earlier for  
353 higher sound frequencies (Figure 2-Figure supplement 1, 2, Figure 4).

354 We verified both of these predictions using electrophysiological recordings from ferret auditory  
355 cortex neurons, fitting STRFs to neuronal responses to sounds from the same rich dataset, and  
356 comparing them to the model kernels. Finally, we used three additional methods - non-adaptive  
357 simulated neurons, probe stimuli and switching stimuli - to confirm that the observed changes in  
358 the neuronal STRFs are consistent with a truly adaptive dynamic process (Figure 3-Figure supple-  
359 ment 2, 3, 4). Thus, our results suggest that the population of auditory cortex neurons adapt to  
360 reverberation by extending their inhibitory field in time in a frequency-dependent manner. This  
361 proposed auditory cortical adaptation is summarized in Figure 5. In the following, we explore these  
362 findings in the broader context of previous studies and possible mechanisms for adaptation to re-  
363 verberation.

## 364 **Auditory cortical neurons adapt their responses to reverberation**

365 Previous studies have shown that human hearing is remarkably robust to reverberation when lis-  
366 teners discriminate speech and naturalistic sounds (*Houtgast and Steeneken, 1985; Bradley, 1986;*  
367 *Darwin and Hukin, 2000; Culling et al., 2003; Nielsen and Dau, 2010*). Our neurophysiological re-  
368 sults in the ferret auditory cortex are consistent with such robust representation. We find that  
369 neurons recorded in the auditory cortex tend to adapt their responses in a way that is consistent  
370 with the computational goal of removing reverberation from natural sounds (Figures 2, 3), even  
371 in anesthetized animals. Our results are also in good agreement with a previous study in awake  
372 passive listening ferrets, which showed that anechoic speech and vocalizations were more read-  
373 ily decodable from the responses of auditory cortex neurons to echoic sounds, than the echoic  
374 sounds themselves (*Mesgarani et al., 2014*). A similar study in humans using EEG corroborated  
375 these findings, showing better decoding accuracy of anechoic speech envelope compared to dis-  
376 torted reverberant speech, but only when listeners attended to the sound sources (*Fuglsang et al.,*  
377 *2017*).

378 Interestingly, a human MEG study suggests that auditory cortex may contain both reverberant  
379 and dereverberated representations of speech in reverberant conditions (*Puvvada et al., 2017*).  
380 In addition, *Traer and McDermott (2016)* found that humans were able to discriminate different  
381 reverberant conditions well with both familiar and unfamiliar sounds. In line with this, a minority  
382 of neurons in our study did not change the timing of their inhibitory responses in different rever-  
383 berant conditions or showed the opposite effect from our model prediction (i.e. their *COM*<sup>-</sup> and  
384 *PT*<sup>-</sup> decreased in the more reverberant room) (Figure 3B,D). Thus, although most cortical neu-  
385 rons adapted to reverberation, it is possible that some of them might carry information about the  
386 reverberant environment or even represent it more explicitly.

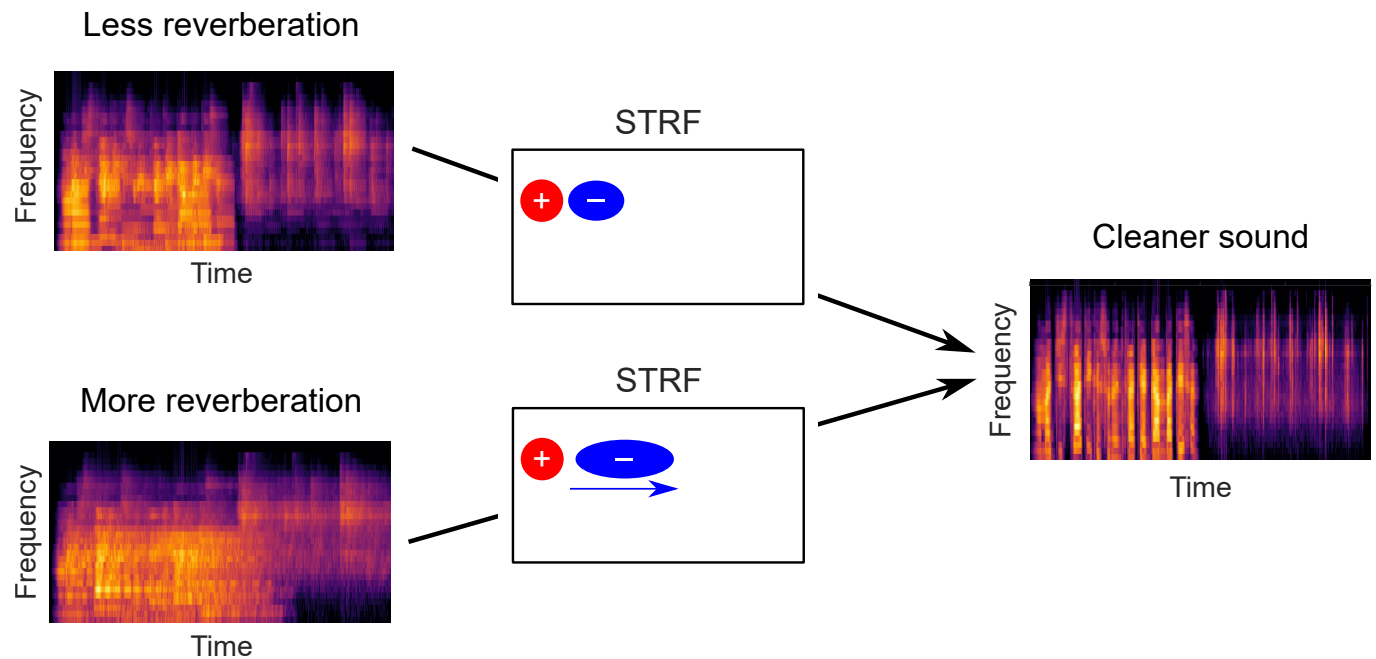


**Figure 5. Schematic of dereverberation by auditory cortex.**

Natural environments contain different levels of reverberation (illustrated by the left cochleograms). Neurons in auditory cortex adjust their inhibitory receptive fields to ameliorate the effects of reverberation, with increased latency of inhibition for more reverberant environments (center). The consequence of this adaptive process is to arrive at a representation of the sound in which reverberation is reduced (right cochleogram).

**387 Temporal shifts in inhibition underlie adaptation to reverberation**

388 Our findings build on and provide an explanation for those of *Mesgarani et al. (2014)*. These au-  
389 thors approximated a reverberant stimulus by convolving speech and vocalizations with decaying  
390 white noise. In contrast, we used a more diverse stimulus set, which included many environmen-  
391 tal sounds that can have very different acoustical statistics (*Attias and Schreiner, 1996; Turner,*  
392 *2010*), and a model of reverberation that included early reflections and their frequency depen-  
393 dence, which are known to have important perceptual effects (*Traer and McDermott, 2016*). *Mes-*  
394 *garani et al. (2014)* proposed a combination of subtractive synaptic depression and multiplicative  
395 gain change as a potential mechanism for the observed adaptation in their study. However, they  
396 acknowledged that other functionally equivalent mechanisms might also be feasible. Notably, their  
397 study did not test different echoic conditions with varying amounts of reverberation. Therefore,  
398 the time constants of the synaptic depression and gain components in their model were fixed.  
399 *Mesgarani et al. (2014)* speculated that these time constants might have an important impact in  
400 conditions with different amounts of reverberation. This is indeed one of our main novel findings:  
401 more reverberant environments require more temporally delayed inhibitory responses within the  
402 STRFs of auditory cortical neurons.

**403 Adaptation to reverberation is frequency dependent**

404 Another novel finding of the present study was that the temporal lag of the inhibition was frequency  
405 dependent in both the model kernels and neuronal STRFs (Figure 2-Figure supplement 1, 2). For  
406 both the small and large rooms, the temporal lag of the inhibition, but not the excitation, approx-  
407 imately tracked the reverberant profile over sound frequency of the acoustic spaces (measured  
408 by the reverberation time ( $RT_{10}$ , Figure 4)). Natural and man-made environments exhibit certain  
409 regularities, and the decline in reverberation over this frequency range is one of them (*Traer and*  
410 *McDermott, 2016*). Future studies could examine whether neurons adapt their responses accord-  
411 ingly to room impulse responses with more unusual  $RT_{10}$  frequency profiles.

412 The frequency-dependence of the delay in inhibition likely relates to some degree to the time  
413 constants of mean-sound-level adaptation (*Dean et al., 2008*), which also decrease with frequency  
414 in inferior colliculus neurons responding to non-reverberant noise stimuli (*Dean et al., 2008*). A  
415 study by *Willmore et al. (2016)* found that this frequency dependence of mean-sound-level adapta-  
416 tion may impact cortical responses and is consistent with removing a running average from natural  
417 sounds with undefined reverberation levels. Hence, the frequency dependence we observe in the  
418 present study may to some extent reflect general mechanisms for removing both reverberation  
419 and the mean sound level, and may be at least partially inherited from subcortical areas.

**420 Possible biological implementations of the adaptation to reverberation**

421 What might be the basis for the cortical adaptation to reverberation that we have observed? Some  
422 plausible mechanisms for altering the inhibitory field include synaptic depression (*David et al.,*  
423 *2009*), intrinsic dynamics of membrane channels (*Abolafia et al., 2011*), hyperpolarizing inputs from  
424 inhibitory neurons (*Li et al., 2015; Natan et al., 2015; Gwak and Kwag, 2020*), or adaptation inher-  
425 ited from subcortical regions such as the inferior colliculus or auditory thalamus (medial geniculate  
426 body) (*Dean et al., 2008; Devore et al., 2009; Willmore et al., 2016; Lohse et al., 2020*). The physio-  
427 logical data obtained in this study do not allow us to discriminate among these mechanisms.

428 Hence, it would be important to investigate whether the adaptive phenomenon we have found  
429 occurs at subcortical levels too, namely the inferior colliculus and the medial geniculate body. Pre-  
430 vious research in the inferior colliculus of rabbits has shown that neural responses to amplitude-  
431 modulated noise partially compensate for background noise and, for some neurons, particularly  
432 when that noise comes from reverberation (*Slama and Delgutte, 2015*). However, this study only  
433 examined one room size, so it did not investigate the temporal phenomenon we observed. *Rabi-*  
434 *nowitz et al. (2013)* found that neurons in the inferior colliculus in ferrets generally adapt less to  
435 the addition of non-reverberant background noise than those recorded in auditory cortex. This

436 and other studies indicate that an increase in adaptation to sound statistics from auditory nerve  
437 to midbrain to cortex helps to construct noise-invariant sound representations in the higher au-  
438 ditory brain (*Dean et al., 2005, 2008; Watkins and Barbour, 2008; Wen et al., 2009; Lohse et al.,*  
439 **2020**). However, subcortical adaptation phenomena may be influenced by cortical activity through  
440 descending connections (*Robinson et al., 2016*), making it challenging to dissect the neuroanatomical  
441 origin of these effects. Similarly, it is possible that reverberation adaptation also becomes more  
442 complete as we progress along the auditory pathway.

443 **Considerations and future work**

444 We undertook our electrophysiological recordings in the present study under general anesthesia  
445 in order to control for the effects of attention on reverberation adaptation and to facilitate stable  
446 recording of neural responses during our large stimulus set. Cortical adaptation to reverberation  
447 has been previously observed in awake listeners ((*Mesgarani et al., 2014; Fuglsang et al., 2017*)),  
448 and we observed adaptive inhibitory plasticity in the anesthetized animal that is also consistent  
449 with dereverberation. This indicates that this form of adaptation is at least in part driven by stim-  
450 ulus statistics and can occur independently of activity and feedback from higher auditory areas  
451 (*Krom et al., 2020*).

452 Previous work has shown no effect of anaesthesia on another kind of adaptation, contrast gain  
453 control, in either the ferret auditory cortex (*Rabinowitz et al., 2011*) or the mouse inferior colliculus  
454 (*Lohse et al., 2020*). There is therefore no *a priori* reason to expect that cortical adaptation to rever-  
455 beration would be substantially different in awake ferrets. Nevertheless, the effects of attention  
456 and behavior on auditory cortical STRFs in the ferret are well documented (*David, 2018*). These  
457 can manifest, for example, as gain changes and tuning shifts. Considering the importance of rever-  
458 beration to perception, it would be interesting to explore the effects described here in behaving  
459 animals.

460 Another point for future research to consider is how our normative model could be further  
461 developed. For simplicity and interpretability, we used an elementary linear model. However, there  
462 are many more complex and powerful models for dereverberation in acoustical engineering, some  
463 of which may provide insight into the biology (*Naylor and Gaubitch, 2010*). Also, in our modelling  
464 we were focused on assessing what characteristics of dereverberation model kernels might change  
465 under different conditions, not on how the brain learns to make these changes. Hence, we gave  
466 our dereverberation model access to the true anechoic sound, something the brain would not have  
467 access to. However, there are blind dereverberation models that aim to dereverberate sounds  
468 from just one or two microphones, without access to the original anechoic sounds or room impulse  
469 response (*Li et al., 2018; Jeub et al., 2010*). These blind dereverberation models will be particu-  
470 larly useful to compare to biology if we want to explore how the brain learns to perform dereverberation  
471 with just two ears. It is also worth considering that the auditory system will be performing other  
472 functions in addition to dereverberation and these may be useful to add into a model.

473 **Summary**

474 We have observed in auditory cortical neurons a form of adaptation where the inhibitory compo-  
475 nent of the receptive fields is delayed in time as the room impulse response increases in a larger  
476 room. This is consistent with the cortex adapting to dereverberate its representation of incoming  
477 sounds in a given acoustic space. Dereverberated representations of sound sources would likely be  
478 more invariant under different acoustic conditions and thus easier to consistently identify and pro-  
479 cess, something valuable for any animal's survival. Reverberation is a ubiquitous phenomenon in  
480 the natural world and provides a substantial challenge to the hearing impaired and speech recogni-  
481 tion technologies. Understanding the adaptive phenomena of the brain that allow us to effortlessly  
482 filter out reverberation may help us to overcome these challenges.

## 483 Methods and Materials

### 484 Animals

485 All animal procedures were approved by the local ethical review committee of the University of  
486 Oxford and performed under license from the UK Home Office. Three adult female and four adult  
487 male ferrets (*Mustela putorius furo*; Marshall BioResources, UK) were used in the electrophysiology  
488 experiments (mean age = 8.4 months; standard deviation = 4.2 months).

### 489 Surgical procedure

490 Terminal electrophysiological recordings were performed on each ferret under general anesthesia.  
491 Anesthesia was induced with an intramuscular injection of ketamine (Vetalar; 5 mg/kg) and  
492 medetomidine (Domitor; 0.02 mg/kg), and was maintained with a continuous intravenous infusion  
493 of these two drugs in Hartmann's solution with 3.5% glucose and dexamethasone (0.5 mg/ml/hr).  
494 The animal was intubated and artificially ventilated with medical O<sub>2</sub>. Respiratory rate, end-tidal CO<sub>2</sub>,  
495 electrocardiogram and blood oxygenation were continuously monitored throughout the recording  
496 session. Eye ointment (Maxitrol; Alcon, UK) was applied throughout and body temperature was  
497 maintained at 36-38°C. Atropine (Atrocare; 0.06 mg/kg i.m.) was administered every 6 hours, or  
498 when bradycardia or arrhythmia was observed.

499 Once anesthetized, each ferret was placed in a custom-built stereotaxic frame and secured with  
500 ear bars and a mouthpiece. After shaving the scalp and injecting bupivacaine (Marcain, <1mg/kg  
501 s.c.), the skin was incised and the left temporal muscle removed. A steel holding bar was secured to  
502 the skull using dental cement (SuperBond; C&B, UK) and a stainless steel bone screw (Veterinary  
503 Instrumentation, UK). A circular craniotomy (10 mm diameter) was drilled over the left auditory  
504 cortex, and the dura was removed in this region. The brain surface was covered with a solution of  
505 1.25% agarose in 0.9% NaCl, and silicone oil was applied to the craniotomy regularly throughout  
506 recording.

507 With the ferret secured in the frame, the ear bars were removed, and the ferret and frame were  
508 placed in an electrically isolated anechoic chamber for recording. Recordings were then carried out  
509 in the left auditory cortex. An Ag/AgCl external reference wire was inserted between the dura and  
510 the skull on the edge of craniotomy. A Neuropixels Phase 3a microelectrode probe (*Jun et al., 2017*)  
511 was inserted orthogonally to the brain surface through the entire depth of auditory cortex.  
512 The cortical area of each penetration was determined based on its anatomical location in the ferret  
513 ectosylvian gyrus, the local field potential response latency, and the frequency response area (FRA)  
514 shapes of neurons. Based on these criteria, 95% of the recorded neurons were either within or on  
515 the ventral border of the primary auditory areas (primary auditory cortex, A1 and anterior auditory  
516 field, AAF), while the remaining neurons were located in secondary fields on the posterior ectosylvian  
517 gyrus. Following each presentation of the complete stimulus set, the probe was moved to a  
518 new location within auditory cortex. Data were acquired at a 30 kHz sampling rate using SpikeGLX  
519 software (<https://github.com/billkarsh/SpikeGLX>) and custom Matlab scripts (Mathworks).

### 520 Spike sorting

521 The recorded signal was processed offline by first digitally highpass filtering at 150Hz. Common av-  
522 erage referencing was performed to remove noise across electrode channels (*Ludwig et al., 2009*).  
523 Spiking activity was then detected and clustered using Kilosort2 software (*Pachitariu et al., 2016*)  
524 (<https://github.com/MouseLand/Kilosort2>). Responses from single neurons were manually curated  
525 using Phy (<https://github.com/cortex-lab/phy>) if they had stereotypical spike shapes with low vari-  
526 ance and their autocorrelation spike histogram showed a clear refractory period. Spikes from a  
527 given cluster were often measurable on 4-6 neighboring electrode channels, facilitating the isolat-  
528 ion of single units. Only well isolated single units and multiunit clusters that were responsive to  
529 the stimuli (noise ratio <40, (*Sahani and Linden, 2003; Rabinowitz et al., 2011*)) were included in  
530 subsequent analyses.

531 **Sound presentation**

532 Stimuli were presented binaurally via Panasonic RP-HV094E-K earphone drivers, coupled to oto-  
533 scope speculae inserted into each ear canal. The speculae were sealed in place with Otoform  
534 (Dreve Otoplastik). The earphones were driven by a System 3 RP2.1 multiprocessor and headphone  
535 amplifier (Tucker-Davis Technologies). Sounds were presented at a sampling rate of 48828Hz. The  
536 output response of the earphones was measured using a Brüel & Kjær calibration system with  
537 a GRAS 40DP microphone coupled to the end of the otoscope speculae with a silicone tube. An  
538 inverse filter was applied to the speaker output to produce a flat spectral response ( $\pm 3\text{dB}$ ) over  
539 the stimulus frequency range (200Hz-22kHz). Sound intensity was calibrated with an Iso-Tech TES-  
540 1356-G sound level calibrator.

541 **Sound stimuli and virtual acoustic space**

542 There are two stimulus sets, the set used to train the dereverberation model, and the set played to  
543 the ferrets, which was prepared from a subset the sounds used to make the first set. The stimuli  
544 used to train the dereverberation model were constructed from a dataset consisting of clips of  
545 anechoic sounds containing human speech and other natural sounds, such as cracking branches,  
546 footsteps, and running water. Most of the sound clips were recorded in an anechoic chamber using  
547 a Zoom H2 or Zoom H4 sound recorder, apart from some that came from the RWCP Sound Scene  
548 Database in Real Acoustic Environments (*Nakamura et al., 1999*). The clips varied in duration from  
549 3s to 10s. A portion of the clips from the dataset was concatenated together to make a single  
550 stimulus of 600s duration. A 0.25s cosine ramp was applied to the onset and offset of each snippet  
551 to avoid clipping artifacts in concatenation. The 600s stimulus was then band-pass filtered from  
552 200Hz-20kHz using an 8th-order Butterworth filter. We also constructed a held-out test set of  
553 100s duration in the same manner using different examples of the same types of sounds from the  
554 dataset.

555 Finally, this stimulus was played in a virtual acoustic space (VAS), providing it with reverberation  
556 and head-related filtering. We used the "Roomsim" software (*Campbell et al., 2005*) to generate  
557 the virtual acoustic space. This software creates a cuboidal room of arbitrary x, y and z dimensions  
558 and simulates its acoustic properties for a listener at a particular position and orientation in space,  
559 for a sound source at a particular position. The simulations are based on the room-image method  
560 (*Allen and Berkley, 1979; Heinz, 1993; Shinn-Cunningham et al., 2001*). One difference between the  
561 standard room-image method and Roomsim is that the latter incorporates the absorption prop-  
562 erties of different materials, which can be summarized by their frequency-dependent absorption  
563 coefficients. In principle, the amount of reverberation in a room will depend on its size, shape and  
564 the material from which the walls are made. For our room simulations the walls, ceiling and floor  
565 use the frequency-dependent absorption coefficients of stone (*Álvarez Morales et al., 2014*). We  
566 decided to vary the amount of reverberation by changing the room size whilst keeping the other  
567 parameters fixed. Four different corridor-shaped rooms were created:

568 1. **Anechoic room**

569 2. **Small room** (length x width x height, 3mx0.3mx0.3m,  $RT_{10} = 130\text{ms}$ )

570 3. **Medium room** (7.5mx0.75mx0.75m,  $RT_{10} = 250\text{ms}$ )

571 4. **Large room** (15mx1.5mx1.5m,  $RT_{10} = 430\text{ms}$ )

572 Thus processing the 600s stimulus for each room provided four 600s stimuli. Note that the ane-  
573 choic room does not have a clearly defined "shape", having no reflecting walls, ceiling or floor, with  
574 the acoustic filtering determined only by the relative orientation and distances of the sound source  
575 and receiver. Roomsim simulates the orientation-specific acoustic properties of the receiver's head  
576 and outer ear, represented by the head-related transfer function (HRTF). In all simulations, we used  
577 the same ferret HRTF provided from measurements previously made in the lab on a real ferret  
578 (from *Schnupp et al., 2001*). The joint filtering properties of the ferret's HRTF and the room were  
579 simulated together by Roomsim to produce a binaural room impulse response (BRIR). The ferret

580 head position and orientation were simulated in the VAS, positioning it 0.15m from the floor, at  
581 the midpoint of the room's width (0.15m for the small, 0.375m for the medium and 0.75m for the  
582 large) and 1/4 of the room's length from one end (0.75m for the small, 1.875m for the medium and  
583 3.75m for the large) and directly facing the opposite end. In all four room conditions, the sound  
584 source was positioned at the same height as the ferret's head (0.15m) and at a distance of 1.5m  
585 straight ahead in the direction faced by the ferret (0° azimuth and 0° elevation relative to the fer-  
586 ret's head). The reverberation time  $RT_{10}$  is the time necessary for the sound level to decay by 10dB  
587 relative to an initial sound impulse. We measured this using a cochlear model, as explained in the  
588 next section *Cochlear model*.

589 The stimuli presented to the ferrets were constructed from a representative subset of the ane-  
590 choic natural stimuli used to train the dereverberation model. We cut 40 different snippets of  
591 natural sounds, each 2s in duration, from the clips in the dataset. These 2s snippets were con-  
592 catenated together into two 40s long stimuli. A 0.25s cosine ramp was applied to the onset and  
593 offset of each snippet to avoid clipping artifacts in concatenation. The two 40s stimulus blocks  
594 were then processed in VAS in exactly the same way as with the modelling stimulus set, for the  
595 same small, medium and large rooms. This provided two 40s blocks for each reverberant condi-  
596 tion (a small, medium or large room, see subsection *Sound stimuli and virtual acoustic space*). We  
597 played the small and large room conditions in 7 animals and the small, medium and large room  
598 conditions in 2 out of those 7. The 40s blocks were presented in pseudo random order, with ~5s  
599 of silence between blocks. This presentation was repeated ten times, with a different order each  
600 time.

### 601 **Cochlear model**

602 We used a power-spectrogram based model of cochlear processing as described in *Rahman et al.*  
603 (2020). Briefly, a spectrogram was produced from the sound waveform by taking the power spec-  
604 trum through a short-time Fourier transform (STFT) using 10-ms Hanning windows, overlapping by  
605 5 ms. The power of adjacent frequency channels was summed using overlapping triangular win-  
606 dows (using code adapted from melbank.m, <http://www.ee.ic.ac.uk/hp/staff/dmb/voicebox/voicebox.html>) to produce 30 log-spaced frequency channels ranging from 400Hz to 19kHz center frequen-  
607 cies. The resulting power in each channel at each time point was converted to log values and any  
608 value below a low threshold was set to that threshold.

609 We used the cochleagram to measure the frequency-band-specific reverberation times ( $RT_{10}$ )  
610 shown in Figure 4C. Our method is similar to that of *Traer and McDermott (2016)*, but for consis-  
611 tency we used our cochlear model rather than theirs. First, we produce an impulse response, the  
612 sound induced at the right ear of the ferret in the virtual room, by a simple click at the standard  
613 source position. Then, we put this impulse response through our cochlear model to generate a  
614 cochleagram. Next, for each frequency band in this cochleagram, we fitted a straight line to the  
615 plot of the decaying log power output (dB) of the cochleagram over time. Using the slope of this line  
616 of best fit, we found the amount of time it took for this output to decay by 10dB. This provided the  
617  $RT_{10}$  for each frequency band. We measured the overall  $RT_{10}$  of each room by taking the median  
618  $RT_{10}$  over all 30 frequency bands.

### 620 **Model kernels**

621 The dereverberation model consisted of a set of linear kernels, one for each of the 30 frequency  
622 channels in the anechoic cochleagram. The kernels were fitted separately for each reverberant  
623 condition, thus providing 30 kernels for each room. The dereverberation model is summarized by  
624 the following equation:

$$\hat{x}_{f't}^{\text{anech}} = \sum_{f=1}^{f_{\max}} \sum_{h=1}^{h_{\max}} k_{f'fh} x_{f(t-h+1)}^{\text{reverb}} + b_{f'} \quad (1)$$

625 Here,  $\hat{x}_{f't}^{\text{anech}}$  is the estimate of the anechoic cochleagram for frequency channel  $f'$  and time bin  
626  $t$ . Obtaining  $\hat{x}_{f't}^{\text{anech}}$  involved convolving the kernels  $k_{f'fh}$  with the reverberant cochleagram  $x_{ft}^{\text{reverb}}$ .  
627 Here  $f$  is the frequency channel in the reverberant cochleagram and  $h$  indexes the time lag used  
628 in the convolutions. The model weights  $k_{f'fh}$  are composed of 30 kernels, one for each frequency  
629 channel  $f'$  in the anechoic cochleagram. Finally, the bias term for frequency channel  $f'$  is  $b_{f'}$ .  
630 For each anechoic frequency channel  $f'$ , the associated model kernel was separately fitted to  
631 minimize the mean squared error between the kernel's estimate of that frequency channel of the  
632 anechoic cochleagram  $\hat{x}_{f't}^{\text{anech}}$  and that actual channel of the anechoic cochleagram  $x_{f't}^{\text{anech}}$ , subject to  
633  $L_2$  regularization ("ridge" regression) on  $k_{f'fh}$ . The weights were fitted using the *glmnet* package  
634 (GLM, J. Qian, T. Hastie, J. Friedman, R. Tibshirani, and N. Simon, Stanford University, Stanford, CA;  
635 [http://web.stanford.edu/~hastie/glmnet\\_matlab/index.html](http://web.stanford.edu/~hastie/glmnet_matlab/index.html)). To select the regularization strength (the  
636 hyperparameter  $\lambda$ ), we performed 10-fold cross-validation, using 90% of the data for the training  
637 set and 10% (an unbroken 60s segment) for the validation set. Our validation sets over folds were  
638 non-overlapping. We found the  $\lambda$  that gave the lowest mean-squared error averaged over the 10  
639 folds. Using this  $\lambda$ , we then re-fitted the model kernels using the whole cross-validation set (training  
640 + validation set). These resulting kernels are the ones shown and used in all analyses. These kernels  
641 were also used to estimate the dereverberation capacity of the model on the held-out test set. Note  
642 that here onward we typically refer to individual model kernels by  $k_{fh}$  for brevity, dropping the  $f'$   
643 index used for the full set of kernels  $k_{f'fh}$ .

#### 644 **Neuronal STRFs**

645 For each cortical unit, for each reverberation condition, we separately estimated its spectro-temporal  
646 receptive field (STRF) using its response to the natural stimuli under that condition (**Theunissen  
647 et al., 2001**). We used the STRF, a linear model, as this enabled comparison to our linear derever-  
648 beration model. The STRF model can be summarized by the following equation:

$$\hat{y}_{nt} = \sum_{f=1}^{f_{\max}} \sum_{h=1}^{h_{\max}} w_{nfh} x_{f(t-h+1)}^{\text{reverb}} + b_n \quad (2)$$

649 Here,  $\hat{y}_{nt}$  is the estimated spike counts of neuron  $n$  at time bin  $t$ . Also,  $x_{ft}^{\text{reverb}}$  is the reverberant  
650 cochleagram in frequency channel  $f$  and at time  $t$ . For each neuron  $n$ , the weights in  $w_{nfh}$  over  
651 frequency channel  $f$  and history (time lag) index  $h$  provide its STRF. Finally,  $b_n$  is the bias term of  
652 unit  $n$ .

653 Notice the similarity of Equation 2 to Equation 1 of the dereverberation model. In both cases,  
654 we used the reverberant cochleagram as an input (from either the small, medium, or large room)  
655 and fitted the best linear mapping to the output. In the case of neuronal STRFs, the output is  
656 the neuronal spike count over time, whereas in the model kernel it is a frequency channel of the  
657 anechoic cochleagram. For each neuron and room, we separately fitted an STRF by minimizing the  
658 mean squared error between the estimated spike counts  $\hat{y}_{nt}$  and the observed spike counts  $y_{nt}$ . To  
659 do this, for a given room, we used the first 36s of neural response to the two 40s-stimuli associated  
660 with that room (as the last 4s contained a noise probe, see subsection Noise burst analysis). The  
661 weights were fitted using the *glmnet* package (GLM, J. Qian, T. Hastie, J. Friedman, R. Tibshirani,  
662 and N. Simon, Stanford University, Stanford, CA; [http://web.stanford.edu/~hastie/glmnet\\_matlab/  
index.html](http://web.stanford.edu/~hastie/glmnet_matlab/<br/>663 index.html)). As for the model kernels (above), the fitting was subject to  $L_2$  regularization. To select  
664 the regularization strength (the hyperparameter  $\lambda$ ), we performed 10-fold cross-validation, using  
665 90% of the data for the training set and 10% (an unbroken 7.2s segment) for the validation set.  
666 Our validation sets over folds were non-overlapping. We found the  $\lambda$  that gave the lowest mean-  
667 squared error averaged over the 10 folds. Using this  $\lambda$ , we then re-fitted the STRFs using the whole  
668 cross-validation set (training + validation set). The resulting STRFs are the ones shown and used in  
669 all analyses. As with the model kernels, from here onwards we typically refer to an individual STRF  
670 for a given neuron by the form  $w_{fh}$  for brevity, dropping the neuron index  $n$  used here in  $w_{nfh}$ .

671 **Quantification of the temporal effects in model kernels and neuronal STRFs**

672 To quantify the temporal profiles of the model kernels and neuronal STRFs, we chose two different  
673 measures:

674 1. Center of mass (*COM*)  
675 2. Peak time (*PT*)

676 To compute them, we first obtained the averaged excitatory and inhibitory temporal profiles  
677 of the model kernels/neuronal STRFs as follows:

$$w_h^+ = \frac{1}{f_{max}} \sum_{f=1}^{f_{max}} [w_{fh}]_+ \quad (3)$$

$$w_h^- = \frac{1}{f_{max}} \sum_{f=1}^{f_{max}} [w_{fh}]_- \quad (4)$$

678 where  $w_{fh}$  is the neuronal STRF with  $f$  and  $h$  subscripts denoting frequency channel and history,  
679 respectively. Equations 3 and 4 are the same for the dereverberation model kernels but with  $k$   
680 instead of  $w$ , as with all subsequent equations in this section.  $f_{max}$  is the number of frequencies  
681 (30) in the model kernel/neuronal STRF  $w_{fh}$ . The notation  $[w_{fh}]_+$  and  $[w_{fh}]_-$  stand for the element-  
682 wise operations  $\max(w_{fh}, 0)$  and  $\min(w_{fh}, 0)$ , that is:

$$[w_{fh}]_+ = \begin{cases} w_{fh} & \text{if } w_{fh} \geq 0 \\ 0 & \text{otherwise} \end{cases} \quad (5)$$

$$[w_{fh}]_- = \begin{cases} w_{fh} & \text{if } w_{fh} \leq 0 \\ 0 & \text{otherwise} \end{cases} \quad (6)$$

683 Thus  $w_h^+$  and  $w_h^-$  are the frequency-averaged positive-only,  $[w_{fh}]_+$ , and negative-only,  $[w_{fh}]_-$ ,  
684 parts of the kernel  $w_{fh}$ .

685 From this, the *COM* was defined as follows:

$$COM^+ = \frac{\tau}{\sum_{h=1}^{h_{max}} w_h^+} \sum_{h=1}^{h_{max}} (h-1) w_h^+ \quad (7)$$

$$COM^- = \frac{\tau}{\sum_{h=1}^{h_{max}} w_h^-} \sum_{h=1}^{h_{max}} (h-1) w_h^- \quad (8)$$

686 The duration of a time bin is  $\tau = 10\text{ms}$ , hence time lag in the history of the neuronal STRF/model  
687 kernel ranges from  $\tau(h-1) = 0\text{ms}$  to  $\tau(h_{max}-1) = 190\text{ms}$ . Thus  $COM^+$  is the temporal center of  
688 mass for the positive (excitatory) components of the neuronal STRF/model kernel and  $COM^-$  the  
689 temporal center of mass for the negative (inhibitory) components.

690 The peak time (*PT*) was defined as the time at which the excitation and inhibition in the fre-  
691 quency averaged neuronal STRFs/model kernels peaked:

$$PT^+ = (\operatorname{argmax}_h (w_h^+) - 1) \tau \quad (9)$$

$$PT^- = (\operatorname{argmin}_h (w_h^-) - 1) \tau \quad (10)$$

692 **Simulated neuron**

693 In order to explore whether the changes that we observed are truly adaptive, we used simulated  
694 neurons that lacked adaptive receptive fields to generate responses. We then applied the same  
695 analyses to these simulated neuronal responses as we did to the actual responses. For each neu-  
696 ron  $n$ , we constructed a corresponding simulated neuron in the following way. First, we fitted a  
697 single STRF as described in section Neuronal STRFs. However, in this case we used the full dataset  
698 from the “small” and “large” conditions together, rather than fitting separate STRFs to the two con-  
699 ditions as we did previously.

700 Next, we fitted a sigmoid output non-linearity by first generating a spike count prediction  $\hat{y}_{nt}$  for  
701 the full dataset according to equation 2 from section Neuronal STRFs, using this single STRF and  
702 then finding the sigmoid that best fits the actual spike count  $y_{nt}$  according to the following equation:

$$\hat{y}_{nt}^{\text{nonlin}} = \frac{\rho_1}{1 + \exp(-(\hat{y}_{nt} - \rho_3)/\rho_2)} + \rho_4 \quad (11)$$

703 Here  $\hat{y}_{nt}^{\text{nonlin}}$  is the output of the point non-linearity at time bin  $t$ , providing a new estimate of  
704 the neuron’s spike count. As mentioned,  $\hat{y}_{nt}$  is the predicted spike count from the linear stage (see  
705 Equation 2) at time bin  $t$ , when fitted to the small and large room responses together. It is the four  
706 parameters  $\rho_1$ ,  $\rho_2$ ,  $\rho_3$  and  $\rho_4$  that are optimized in the fit.

707 We then used the fitted simulated model to produce an approximation of the real neuronal  
708 response to the reverberant stimulus sets for both the small and large conditions. In order to sim-  
709 ulate realistic neuronal noise, we used the  $\hat{y}_{nt}^{\text{nonlin}}$  output, at each time bin  $t$ , as the mean of a Poisson  
710 distribution from which we generated 10 “virtual” trials. Finally we performed the same analyses  
711 on these simulated neural responses as we did for the real data; we fitted STRFs for the two re-  
712 verberation conditions separately using these simulated model responses in place of the actual  
713 responses and then analyzed the resulting STRFs as outlined in the section above (Quantification  
714 of the temporal effects in model kernels and neuronal STRFs).

715 **Noise burst analysis**

716 To further confirm the adaptive change in properties of neurons across the two reverberant condi-  
717 tions, we presented a 500ms long unverberated broadband noise burst embedded at a random  
718 time in the last 4s of each 40s sound block (i.e., from 36-40s) for each condition (small and large).  
719 Seven out of the ten repeats of any stimulus block contained a noise burst, with those seven ran-  
720 domly shuffled within the ten. The random timing distribution of the noise bursts was uniform  
721 and independent across repeats and conditions. For each neuron, responses to the noise bursts  
722 were assessed using peristimulus time histogram (PSTHs) with 10ms time bins. For the majority  
723 of neurons, the firing rate had returned to baseline by 100ms, so we decided to use the 0-100ms  
724 time window for further analysis (Figure 3-Figure supplement 3A). Different neurons had different  
725 response profiles, so in order to compare the adaptive properties in the two conditions we chose  
726 the center of mass (*COM*) of the firing rate profile within this window as a robust measure. This  
727 was defined similarly to the *COM* measure in subsection Quantification of the temporal effects in  
728 model kernels and neuronal STRFs (see also Equations 7 and 8). The *COM* for the noise bursts  
729 in the large and small conditions was calculated for each neuron individually and the difference  
730 between the two conditions computed (Figure 3-Figure supplement 3B).

731 **Switching stimuli analysis**

732 In order to confirm and explore the adaptive nature of the neuronal responses to reverberant  
733 sounds, we presented “switching stimuli” (Figure 3-Figure supplement 4A). These stimuli switched  
734 back and forth every 8 seconds between the large room and the small room and were created in the  
735 following way. First, we took our original reverberant stimuli for both the small room (80s duration)  
736 and large room (80s duration) conditions and divided them into consecutive 4s snippets, providing  
737 20 snippets for each condition. We duplicated these two sets and shuffled each one independently,

738 providing a total of four sets of 20 4s-long snippets. We then combined the snippets into eight 40s-  
739 long switching stimuli. These switching stimuli comprised 5 epochs of 8s duration each, with 4  
740 "switches" between the small and large epochs. Half of the stimuli started from the large room  
741 condition and the other half from the small room condition. Within each 8s epoch, we defined two  
742 periods (period 1: 0-4s and period 2: 4-8s). The large-room periods were denoted by L1 (0-4s) and  
743 L2 (4-8s), and the small-room periods by S1 (0-4s) and S2 (4-8s) (Figure 3-Figure supplement 4A).  
744 The snippets from the first small-room set of 20 snippets populated the 20 S1 periods in order,  
745 while those from the second small-room set populated the S2 periods in a different order, due  
746 to the shuffling. Likewise, snippets from the first large-room set of 20 snippets populated the 20  
747 L1 periods, and those from the second large-room set populated the L2 periods. Thus, the same  
748 set of stimuli were included in S1 and S2, and in L1 and L2, with the only differences being their  
749 ordering, and between the small and large room stimuli the amount of reverberation. When the 4s  
750 periods and 8s epochs were spliced together, they were cross-faded into each other with a 10ms  
751 cosine ramp with 5ms overlap, such that the transition from one period to the next was smooth  
752 with no detectable clicks between them. We played the eight 40s stimuli in random order to the  
753 ferrets; this was repeated 10 times with the order different each time.

754 The cortical responses recorded with these stimuli were analyzed using the procedure outlined  
755 in subsection *Neuronal STRFs*. For each neuron, we fitted four separate STRFs using the neural  
756 responses to the S1, S2, L1 and L2 periods. We did not use the first 8s of each of the eight 40s  
757 stimuli, since there was no prior sound (silence) and thus they would not be directly comparable  
758 to the other 4 epochs. We also did not use the first 500 ms of any of the periods, to avoid potential  
759 non-reverberation-related responses from the rapid transitions between them. From the resulting  
760 four STRFs, we extracted the *COM<sup>+</sup>* and *COM<sup>-</sup>* values for each and compared S1 to S2 (Figure 3-  
761 Figure supplement 4B) and L1 to L2 (Figure 3-Figure supplement 4C).

## 762 Acknowledgments

763 We are grateful to Dr Quentin Gaucher for assistance with these electrophysiological experiments.  
764 We would also like to thank Zlatina Dimitrova for her artwork in Figure 1. This work was supported  
765 by a Wellcome Principal Research Fellowship to AJK (WT108369/Z/2015/Z), a BBSRC New Investi-  
766 gator Award (BB/M010929/1) to KMMW, and a Christopher Welch Scholarship (Oxford University  
767 Press) to AZI.

## 768 References

769 **Abolafia JM**, Vergara R, Arnold MM, Reig R, Sanchez-Vives MV. Cortical Auditory Adaptation in the Awake Rat  
770 and the Role of Potassium Currents. *Cerebral Cortex*. 2011 May; 21(5):977–990. <https://academic.oup.com/cercor/article-lookup/doi/10.1093/cercor/bhq163>, doi: 10.1093/cercor/bhq163.

772 **Allen JB**, Berkley DA. Image method for efficiently simulating small-room acoustics. *The Journal of the  
773 Acoustical Society of America*. 1979 Apr; 65(4):943–950. <https://asa.scitation.org/doi/10.1121/1.382599>, doi:  
774 10.1121/1.382599, publisher: Acoustical Society of America.

775 **Attias H**, Schreiner CE. Temporal Low-Order Statistics of Natural Sounds. In: *NIPS*; 1996. .

776 **Bizley JK**, Nodal FR, Nelken I, King AJ. Functional organization of ferret auditory cortex. *Cerebral Cortex*.  
777 2005; 15(10):1637–1653. [http://www.ncbi.nlm.nih.gov/entrez/query.fcgi?cmd=Retrieve&db=PubMed&dopt=Citation&list\\_uids=15703254](http://www.ncbi.nlm.nih.gov/entrez/query.fcgi?cmd=Retrieve&db=PubMed&dopt=Citation&list_uids=15703254).

779 **Bradley JS**. Speech intelligibility studies in classrooms. *The Journal of the Acoustical Society of America*. 1986  
780 Sep; 80(3):846–854. <http://asa.scitation.org/doi/10.1121/1.393908>, doi: 10.1121/1.393908.

781 **Brown GJ**, Cooke M. Computational auditory scene analysis. *Computer Speech & Language*. 1994 Oct; 8(4):297–  
782 336. <http://www.sciencedirect.com/science/article/pii/S0885230884710163>, doi: 10.1006/csla.1994.1016.

783 **Brughera A**, Mikiel-Hunter J, Dietz M, McAlpine D. Auditory brainstem models: adapting cochlear nuclei  
784 improve spatial encoding by the medial superior olive in reverberation. *bioRxiv*. 2020 Jan; p. 694356.  
785 <http://biorxiv.org/content/early/2020/03/27/694356.abstract>, doi: 10.1101/694356.

786 **Campbell DR**, Palomaki KJ, Brown G. A MATLAB simulation of "shoebox" room acoustics for use in research  
787 and teaching. *Computing and Information Systems J*. 2005; 9:48–51.

788 **Christianson GB**, Sahani M, Linden JF. The Consequences of Response Nonlinearities for Interpretation of  
789 Spectrotemporal Receptive Fields. *Journal of Neuroscience*. 2008 Jan; 28(2):446–455. <https://www.jneurosci.org/lookup/doi/10.1523/JNEUROSCI.1775-07.2007>, doi: 10.1523/JNEUROSCI.1775-07.2007.

790 **Culling JF**, Hodder KI, Toh CY. Effects of reverberation on perceptual segregation of competing voices. *The Journal of the Acoustical Society of America*. 2003; 114(5):2871. <http://scitation.aip.org/content/asa/journal/jasa/114/5/10.1121/1.1616922>, doi: 10.1121/1.1616922.

791 **Culling JF**, Summerfield Q, Marshall DH. Effects of simulated reverberation on the use of binaural cues and  
792 fundamental-frequency differences for separating concurrent vowels. *Speech Communication*. 1994 Feb;  
793 14(1):71–95. doi: 10.1016/0167-6393(94)90058-2.

794 **Darwin CJ**, Hukin RW. Effects of reverberation on spatial, prosodic, and vocal-tract size cues to selective attention. *The Journal of the Acoustical Society of America*. 2000 Jul; 108(1):335–342. <http://asa.scitation.org/doi/10.1121/1.429468>, doi: 10.1121/1.429468.

795 **David SV**, Mesgarani N, Fritz JB, Shamma SA. Rapid Synaptic Depression Explains Nonlinear Modulation  
796 of Spectro-Temporal Tuning in Primary Auditory Cortex by Natural Stimuli. *Journal of Neuroscience*.  
797 2009 Mar; 29(11):3374–3386. <http://www.jneurosci.org/cgi/doi/10.1523/JNEUROSCI.5249-08.2009>, doi: 10.1523/JNEUROSCI.5249-08.2009.

798 **David SV**. Incorporating behavioral and sensory context into spectro-temporal models of auditory encoding. *Hearing Research*. 2018 Mar; 360:107–123. <https://linkinghub.elsevier.com/retrieve/pii/S0378595517303611>, doi: 10.1016/j.heares.2017.12.021.

799 **Dean I**, Harper NS, McAlpine D. Neural population coding of sound level adapts to stimulus statistics. *Nature neuroscience*. 2005; 8(12):1684–1689. doi: 10.1038/nn1541, ISBN: 1097-6256 (Print).

800 **Dean I**, Robinson BL, Harper NS, McAlpine D. Rapid neural adaptation to sound level statistics. *J Neurosci*.  
801 2008; 28(25):6430–6438. doi: 10.1523/JNEUROSCI.0470-08.2008, ISBN: 1529-2401 (Electronic) r0270-6474  
802 (Linking).

803 **deCharms RC**, Blake DT, Merzenich MM. Optimizing Sound Features for Cortical Neurons. *Science*. 1998  
804 May; 280(5368):1439–1444. <https://www.science.org/doi/10.1126/science.280.5368.1439>, doi: 10.1126/science.280.5368.1439.

805 **Devore S**, Ihlefeld A, Hancock K, Shinn-Cunningham B, Delgutte B. Accurate Sound Localization in Re-  
806 reverberant Environments Is Mediated by Robust Encoding of Spatial Cues in the Auditory Midbrain.  
807 *Neuron*. 2009 Apr; 62(1):123–134. <https://linkinghub.elsevier.com/retrieve/pii/S0896627309001639>, doi: 10.1016/j.neuron.2009.02.018.

808 **Fitzpatrick DC**, Kuwada S, Kim DO, Parham K, Batra R. Responses of neurons to click-pairs as simulated echoes:  
809 Auditory nerve to auditory cortex. *The Journal of the Acoustical Society of America*. 1999 Dec; 106(6):3460–  
810 3472. <http://asa.scitation.org/doi/10.1121/1.428199>, doi: 10.1121/1.428199.

811 **Fuglsang SA**, Dau T, Hjortkjær J. Noise-robust cortical tracking of attended speech in real-world acoustic scenes. *NeuroImage*. 2017 Aug; 156:435–444. <https://linkinghub.elsevier.com/retrieve/pii/S105381191730318X>, doi: 10.1016/j.neuroimage.2017.04.026.

812 **Guediche S**, Blumstein SE, Fiez JA, Holt LL. Speech perception under adverse conditions: insights from behav-  
813 ioral, computational, and neuroscience research. *Frontiers in Systems Neuroscience*. 2014; 7(4):328–32. doi:  
814 10.3389/fnsys.2013.00126.

815 **Gwak J**, Kwag J. Distinct subtypes of inhibitory interneurons differentially promote the propagation of rate and  
816 temporal codes in the feedforward neural network. *Chaos: An Interdisciplinary Journal of Nonlinear Science*.  
817 2020 May; 30(5):053102. <http://aip.scitation.org/doi/10.1063/1.5134765>, doi: 10.1063/1.5134765.

818 **Harper NS**, Schoppe O, Willmore BDB, Cui Z, Schnupp JWH, King AJ. Network Receptive Field Modeling Reveals  
819 Extensive Integration and Multi-feature Selectivity in Auditory Cortical Neurons. *PLOS Computational Biology*.  
820 2016 Nov; 12(11):e1005113. <https://journals.plos.org/ploscompbiol/article?id=10.1371/journal.pcbi.1005113>, publisher: Public Library of Science.

821 **Hartmann WM**. Localization of sound in rooms. *The Journal of the Acoustical Society of America*. 1982 Nov;  
822 72(S1):S93–S93. <http://asa.scitation.org/doi/10.1121/1.2020159>, doi: 10.1121/1.2020159.

837 **Heinz R.** Binaural room simulation based on an image source model with addition of statistical methods to  
838 include the diffuse sound scattering of walls and to predict the reverberant tail. *Applied Acoustics*. 1993  
839 Jan; 38(2):145–159. <http://www.sciencedirect.com/science/article/pii/0003682X9390048B>, doi: 10.1016/0003-  
840 682X(93)90048-B.

841 **Helper KS**, Wilber LA. Hearing loss, aging, and speech perception in reverberation and noise. *Journal of speech  
842 and hearing research*. 1990 Mar; 33(1):149–55.

843 **Houtgast T**, Steeneken HJM. A review of the MTF concept in room acoustics and its use for estimating speech  
844 intelligibility in auditoria. *The Journal of the Acoustical Society of America*. 1985 Mar; 77(3):1069–1077. <http://asa.scitation.org/doi/10.1121/1.392224>, doi: 10.1121/1.392224.

846 **Huisman WHT**, Attenborough K. Reverberation and attenuation in a pine forest. *The Journal of the Acous-  
847 tical Society of America*. 1991 Nov; 90(5):2664–2677. <http://asa.scitation.org/doi/10.1121/1.401861>, doi:  
848 10.1121/1.401861.

849 **Humes LE**, Dirks DD, Bell TS, Ahlstrom C, Kincaid GE. Application of the Articulation Index and the Speech  
850 Transmission Index to the recognition of speech by normal-hearing and hearing-impaired listeners. *Journal  
851 of speech and hearing research*. 1986 Dec; 29(4):447–62.

852 **Jeub M**, Löllmann HW, Vary P. Blind Dereverberation for Hearing Aids with Binaural Link. In: Bochum; 2010.  
853 p. 4. <http://ikspub.iks.rwth-aachen.de/pdfs/jeub10c.pdf>.

854 **Jun JJ**, Steinmetz NA, Siegle JH, Denman DJ, Bauza M, Barbarits B, Lee AK, Anastassiou CA, Andrei A, Aydin Barbic  
855 M, Blanche TJ, Bonin V, Couto J, Dutta B, Gratton SL, Gutnisky DA, Häusser M, Karsh B, Ledochowitsch P, et al.  
856 Fully integrated silicon probes for high-density recording of neural activity. *Nature*. 2017 Nov; 551(7679):232–  
857 236. <http://www.nature.com/articles/nature24636>, doi: 10.1038/nature24636.

858 **Kell AJE**, McDermott JH. Invariance to background noise as a signature of non-primary auditory cortex.  
859 *Nature Communications*. 2019 Dec; 10(1):3958. <http://www.nature.com/articles/s41467-019-11710-y>, doi:  
860 10.1038/s41467-019-11710-y.

861 **Khalighinejad B**, Herrero JL, Mehta AD, Mesgarani N. Adaptation of the human auditory cortex to chang-  
862 ing background noise. *Nature Communications*. 2019 Dec; 10(1):2509. <http://www.nature.com/articles/s41467-019-10611-4>, doi: 10.1038/s41467-019-10611-4.

864 **Kim DO**, Zahorik P, Carney LH, Bishop BB, Kuwada S. Auditory Distance Coding in Rabbit Midbrain Neu-  
865 rons and Human Perception: Monaural Amplitude Modulation Depth as a Cue. *Journal of Neuroscience*.  
866 2015 Apr; 35(13):5360–5372. <http://www.jneurosci.org/cgi/doi/10.1523/JNEUROSCI.3798-14.2015>, doi:  
867 10.1523/JNEUROSCI.3798-14.2015.

868 **Kinoshita K**, Delcroix M, Gannot S, P Habets EA, Haeb-Umbach R, Kellermann W, Leutnant V, Maas R, Nakatani  
869 T, Raj B, Sehr A, Yoshioka T. A summary of the REVERB challenge: state-of-the-art and remaining chal-  
870 lenges in reverberant speech processing research. *EURASIP Journal on Advances in Signal Processing*.  
871 2016 Dec; 2016(1):7. <https://asp-eurasipjournals.springeropen.com/articles/10.1186/s13634-016-0306-6>, doi:  
872 10.1186/s13634-016-0306-6.

873 **Knudsen VO**. The hearing of speech in auditoriums. *The Journal of the Acoustical Society of America*. 1929;  
874 1(1):56. doi: 10.1121/1.1901470.

875 **Kolarik AJ**, Moore BCJ, Cirstea S, Aggius-Vella E, Gori M, Campus C, Pardhan S. Factors Affecting Auditory  
876 Estimates of Virtual Room Size: Effects of Stimulus, Level, and Reverberation. *Perception*. 2021 Jul; 50(7):646–  
877 663. <http://journals.sagepub.com/doi/10.1177/03010066211020598>, doi: 10.1177/03010066211020598.

878 **Krom AJ**, Marmelshtein A, Gelbard-Sagiv H, Tankus A, Hayat H, Hayat D, Matot I, Strauss I, Fahoum F, Soehle M,  
879 Boström J, Mormann F, Fried I, Nir Y. Anesthesia-induced loss of consciousness disrupts auditory responses  
880 beyond primary cortex. *Proceedings of the National Academy of Sciences*. 2020 May; 117(21):11770–11780.  
881 <http://www.pnas.org/lookup/doi/10.1073/pnas.1917251117>, doi: 10.1073/pnas.1917251117.

882 **Kuttruff H**. Room acoustics. Sixth edition ed. Boca Raton: CRC Press/Taylor & Francis Group; 2017.

883 **Kuwada S**, Bishop B, Kim DO. Approaches to the study of neural coding of sound source location and sound  
884 envelope in real environments. *Frontiers in Neural Circuits*. 2012; 6. <http://journal.frontiersin.org/article/10.3389/fncir.2012.00042/abstract>, doi: 10.3389/fncir.2012.00042.

886 **Li C**, Wang T, Xu S, Xu B. Single-channel Speech Dereverberation via Generative Adversarial Training.  
887 arXiv:180609325 [cs, eess]. 2018 Jun; <http://arxiv.org/abs/1806.09325>, arXiv: 1806.09325.

888 **Li Ly**, Xiong XR, Ibrahim LA, Yuan W, Tao HW, Zhang Li. Differential Receptive Field Properties of Parvalbumin  
889 and Somatostatin Inhibitory Neurons in Mouse Auditory Cortex. *Cerebral Cortex*. 2015 Jul; 25(7):1782–1791.  
890 <https://academic.oup.com/cercor/article-lookup/doi/10.1093/cercor/bht417>, doi: 10.1093/cercor/bht417.

891 **Linden JF**, Liu RC, Sahani M, Schreiner CE, Merzenich MM. Spectrotemporal Structure of Receptive Fields in  
892 Areas AI and AAF of Mouse Auditory Cortex. *Journal of Neurophysiology*. 2003 Oct; 90(4):2660–2675. <https://journals.physiology.org/doi/full/10.1152/jn.00751.2002>, doi: 10.1152/jn.00751.2002, publisher: American  
893 Physiological Society.

894

895 **Litovsky RY**, Yin TCT. Physiological Studies of the Precedence Effect in the Inferior Colliculus of the Cat. I.  
896 Correlates of Psychophysics. *Journal of Neurophysiology*. 1998 Sep; 80(3):1285–1301. <https://www.physiology.org/doi/10.1152/jn.1998.80.3.1285>, doi: 10.1152/jn.1998.80.3.1285.

897

898 **Lohse M**, Bajo VM, King AJ, Willmore BDB. Neural circuits underlying auditory contrast gain control and their  
899 perceptual implications. *Nature Communications*. 2020 Dec; 11(1):324. <http://www.nature.com/articles/s41467-019-14163-5>, doi: 10.1038/s41467-019-14163-5.

900

901 **Ludwig KA**, Miriani RM, Langhals NB, Joseph MD, Anderson DJ, Kipke DR. Using a Common Average Reference  
902 to Improve Cortical Neuron Recordings From Microelectrode Arrays. *Journal of Neurophysiology*. 2009 Mar;  
903 101(3):1679–1689. <https://www.physiology.org/doi/10.1152/jn.90989.2008>, doi: 10.1152/jn.90989.2008.

904

905 **Mesgarani N**, David SV, Fritz JB, Shamma SA. Mechanisms of noise robust representation of speech in primary  
906 auditory cortex. *Proceedings of the National Academy of Sciences*. 2014 May; 111(18):6792–6797. <http://www.pnas.org/cgi/doi/10.1073/pnas.1318017111>, doi: 10.1073/pnas.1318017111.

907

908 **Moore RC**, Lee T, Theunissen FE. Noise-invariant Neurons in the Avian Auditory Cortex: Hearing the Song  
909 in Noise. *PLoS Computational Biology*. 2013 Mar; 9(3):e1002942. <https://dx.plos.org/10.1371/journal.pcbi.1002942>, doi: 10.1371/journal.pcbi.1002942.

910

911 **Álvarez Morales L**, Zamarreño T, Girón S, Galindo M. A methodology for the study of the acoustic environment  
912 of Catholic cathedrals: Application to the Cathedral of Malaga. *Building and Environment*. 2014 Feb; 72:102–  
115. <https://linkinghub.elsevier.com/retrieve/pii/S0360132313003065>, doi: 10.1016/j.buildenv.2013.10.015.

913

914 **Nakamura S**, Hiyane K, Asano F, Endo T. Sound scene data collection in real acoustical environments. *Journal  
915 of the Acoustical Society of Japan (E)*. 1999; 20(3):225–231. [http://www.jstage.jst.go.jp/article/ast1980/20/3/20\\_3\\_225/\\_article](http://www.jstage.jst.go.jp/article/ast1980/20/3/20_3_225/_article), doi: 10.1250/ast.20.225.

916

917 **Natan RG**, Briguglio JJ, Mwilambwe-Tshilobo L, Jones SI, Aizenberg M, Goldberg EM, Geffen MN. Complementary  
918 control of sensory adaptation by two types of cortical interneurons. *eLife*. 2015 Oct; 4:e09868. <https://elifesciences.org/articles/09868>, doi: 10.7554/eLife.09868.

919

920 **Naylor PA**, Gaubitch ND. Speech Dereverberation. Springer Science & Business Media; 2010. <https://www.springer.com/gp/book/9781849960557>.

921

922 **Nielsen JB**, Dau T. Revisiting perceptual compensation for effects of reverberation in speech identification.  
923 The Journal of the Acoustical Society of America. 2010 Nov; 128(5):3088–3094. <http://asa.scitation.org/doi/10.1121/1.3494508>, doi: 10.1121/1.3494508.

924

925 **Nábělek AK**, Letowski TR, Tucker FM. Reverberant overlap- and self-masking in consonant identification. *The  
Journal of the Acoustical Society of America*. 1989 Oct; 86(4):1259–65.

926

927 **Pachitariu M**, Steinmetz N, Kadir S, Carandini M, Harris KD. Kilosort: realtime spike-sorting for extracellular  
928 electrophysiology with hundreds of channels. *bioRxiv*. 2016; p. 061481. <http://biorxiv.org/lookup/doi/10.1101/061481>, doi: 10.1101/061481.

929

930 **Pecka M**, Zahn TP, Saunier-Rebori B, Siveke I, Felmy F, Wiegreb L, Klug A, Pollak GD, Grothe B. Inhibiting  
931 the Inhibition: A Neuronal Network for Sound Localization in Reverberant Environments. *Journal of Neuro-  
932 science*. 2007 Feb; 27(7):1782–1790. <http://www.jneurosci.org/cgi/doi/10.1523/JNEUROSCI.5335-06.2007>, doi: 10.1523/JNEUROSCI.5335-06.2007.

933

934 **Poissant SF**, Whitmal NA, Freyman RL. Effects of reverberation and masking on speech intelligibility in cochlear  
935 implant simulations. *The Journal of the Acoustical Society of America*. 2006 Mar; 119(3):1606–15.

936

937 **Puvvada KC**, Villafañe-Delgado M, Brodbeck C, Simon JZ. Neural Coding of Noisy and Reverberant Speech in  
938 Human Auditory Cortex. *bioRxiv*. 2017 Jan; p. 229153. <http://biorxiv.org/content/early/2017/12/04/229153.abstract>, doi: 10.1101/229153.

938 **Qin MK**, Oxenham AJ. Effects of envelope-vocoder processing on F0 discrimination and concurrent-vowel iden-  
939 tification. *Ear and hearing*. 2005 Oct; 26(5):451–60.

940 **Rabinowitz NC**, Willmore BDB, King AJ, Schnupp JWH. Constructing Noise-Invariant Representations of Sound  
941 in the Auditory Pathway. *PLoS Biology*. 2013; 11(11):e1001710. doi: [10.1371/journal.pbio.1001710](https://doi.org/10.1371/journal.pbio.1001710).

942 **Rabinowitz N**, Willmore BB, Schnupp JH, King A. Contrast Gain Control in Auditory Cortex. *Neuron*. 2011;  
943 70(6):1178–1191. doi: [10.1016/j.neuron.2011.04.030](https://doi.org/10.1016/j.neuron.2011.04.030), publisher: Elsevier Inc.

944 **Rahman M**, Willmore BDB, King AJ, Harper NS. A dynamic network model of temporal receptive fields in pri-  
945 mary auditory cortex. *PLOS Computational Biology*. 2019 May; 15(5):e1006618. <https://journals.plos.org/ploscompbiol/article?id=10.1371/journal.pcbi.1006618>, doi: [10.1371/journal.pcbi.1006618](https://doi.org/10.1371/journal.pcbi.1006618), publisher: Public  
946 Library of Science.

947

948 **Rahman M**, Willmore BDB, King AJ, Harper NS. Simple transformations capture auditory input to cortex. Pro-  
949 ceedings of the National Academy of Sciences. 2020 Nov; 117(45):28442–28451. <http://www.pnas.org/lookup/doi/10.1073/pnas.1922033117>, doi: [10.1073/pnas.1922033117](https://doi.org/10.1073/pnas.1922033117).

950

951 **Rakerd B**, Hartmann WM. Localization of noise in a reverberant environment. In: Pressnitzer D, de Cheveigné  
952 A, McAdams S, Collet L, editors. *Auditory Signal Processing* New York, NY: Springer New York; 2005.p. 413–421.  
953 [http://link.springer.com/10.1007/0-387-27045-0\\_51](http://link.springer.com/10.1007/0-387-27045-0_51), doi: [10.1007/0-387-27045-0\\_51](https://doi.org/10.1007/0-387-27045-0_51).

954 **Robinson BL**, Harper NS, McAlpine D. Meta-adaptation in the auditory midbrain under cortical influ-  
955 ence. *Nature Communications*. 2016 Dec; 7(1):13442. <http://www.nature.com/articles/ncomms13442>, doi:  
956 [10.1038/ncomms13442](https://doi.org/10.1038/ncomms13442).

957 **Sahani M**, Linden JF. How Linear are Auditory Cortical Responses? In: Becker S, Thrun S, Obermayer K, editors.  
958 *Advances in Neural Information Processing Systems 15* MIT Press; 2003.p. 125–132. <http://papers.nips.cc/paper/2335-how-linear-are-auditory-cortical-responses.pdf>.

959

960 **Sakai H**, Sato Si, Ando Y. Orthogonal acoustical factors of sound fields in a forest compared with those in  
961 a concert hall. *The Journal of the Acoustical Society of America*. 1998 Sep; 104(3):1491–1497. <http://asa.scitation.org/doi/10.1121/1.424360>, doi: [10.1121/1.424360](https://doi.org/10.1121/1.424360).

961

962

963 **Sayles M**, Winter IM. Reverberation Challenges the Temporal Representation of the Pitch of Complex  
964 Sounds. *Neuron*. 2008 Jun; 58(5):789–801. <https://linkinghub.elsevier.com/retrieve/pii/S0896627308003036>,  
965 doi: [10.1016/j.neuron.2008.03.029](https://doi.org/10.1016/j.neuron.2008.03.029).

966

967 **Schnupp JW**, Mrsic-Flogel TD, King AJ. Linear processing of spatial cues in primary auditory cortex. *Nature*.  
2001 Nov; 414(6860):200–204. doi: [10.1038/35102568](https://doi.org/10.1038/35102568).

968

969 **Schwartz O**, Pillow JW, Rust NC, Simoncelli EP. Spike-triggered neural characterization. *Journal of Vision*. 2006  
Jul; 6(4):13. <http://jov.arvojournals.org/article.aspx?doi=10.1167/6.4.13>, doi: [10.1167/6.4.13](https://doi.org/10.1167/6.4.13).

970

971 **Schweitzer HC**. Reducing the Negative Effects of Reverberation in Hearing Aid Processing. *Hear-  
972 ing Review*. 2003 Nov; p. 1–5. <https://www.hearingreview.com/hearing-products/accessories/components/reducing-the-negative-effects-of-reverberation-in-hearing-aid-processing>.

973

974 **Shinn-Cunningham B**, Kawakyu K. Neural representation of source direction in reverberant space. In: *2003  
975 IEEE Workshop on Applications of Signal Processing to Audio and Acoustics (IEEE Cat. No.03TH8684)* New Paltz, NY,  
976 USA: IEEE; 2003. p. 79–82. <http://ieeexplore.ieee.org/document/1285824/>, doi: [10.1109/ASPA.2003.1285824](https://doi.org/10.1109/ASPA.2003.1285824).

977

978 **Shinn-Cunningham B**. Learning Reverberation: Considerations for Spatial Auditory Displays. *Proceedings of  
979 the 2000 International Conference on Auditory Display*. 2000; (April):126–134. doi: [10.1.1.22.5056](https://doi.org/10.1.1.22.5056).

980

981 **Shinn-Cunningham BG**, Lin IF, Streeter T. Trading Directional Accuracy for Realism in a Virtual Auditory Dis-  
play. In: Las Vegas; 2005. p. 11. [https://www.cmu.edu/dietrich/psychology/shinn/publications/pdfs/2005/2005vrinthcii\\_shinn.pdf](https://www.cmu.edu/dietrich/psychology/shinn/publications/pdfs/2005/2005vrinthcii_shinn.pdf).

982

983 **Shinn-Cunningham BG**, Desloge JG, Kopco N. Empirical and modeled acoustic transfer functions in a simple  
984 room: effects of distance and direction. In: *Proceedings of the 2001 IEEE Workshop on the Applications of  
985 Signal Processing to Audio and Acoustics (Cat. No.01TH8575)* New Platz, NY, USA: IEEE; 2001. p. 183–186. <http://ieeexplore.ieee.org/document/969573/>, doi: [10.1109/ASPA.2001.969573](https://doi.org/10.1109/ASPA.2001.969573).

986

985 **Singer Y**, Teramoto Y, Willmore BD, Schnupp JW, King AJ, Harper NS. Sensory cortex is optimized for prediction  
986 of future input. *eLife*. 2018; 7. doi: [10.7554/eLife.31557](https://doi.org/10.7554/eLife.31557).

987 Slama MCC, Delgutte B. Neural Coding of Sound Envelope in Reverberant Environments. *Journal of Neuroscience*. 2015 Mar; 35(10):4452-4468. <http://www.jneurosci.org/cgi/doi/10.1523/JNEUROSCI.3615-14.2015>, doi: 10.1523/JNEUROSCI.3615-14.2015.

990 Spitzer MW, Bala ADS, Takahashi TT. A Neuronal Correlate of the Precedence Effect Is Associated With Spatial Selectivity in the Barn Owl's Auditory Midbrain. *Journal of Neurophysiology*. 2004 Oct; 92(4):2051-2070. <https://www.physiology.org/doi/10.1152/jn.01235.2003>, doi: 10.1152/jn.01235.2003.

993 Theunissen FE, David SV, Singh NC, Hsu A, Vinje WE, Gallant JL. Estimating spatio-temporal receptive fields of auditory and visual neurons from their responses to natural stimuli. *Network: Computation in Neural Systems*. 2001 Jan; 12(3):289-316. <https://doi.org/10.1080/net.12.3.289.316>, doi: 10.1080/net.12.3.289.316, publisher: Taylor & Francis \_eprint: <https://doi.org/10.1080/net.12.3.289.316>.

997 Tollin DJ, Populin LC, Yin TCT. Neural Correlates of the Precedence Effect in the Inferior Colliculus of Behaving Cats. *Journal of Neurophysiology*. 2004 Dec; 92(6):3286-3297. <https://www.physiology.org/doi/10.1152/jn.00606.2004>, doi: 10.1152/jn.00606.2004.

1000 Traer J, McDermott JH. Statistics of natural reverberation enable perceptual separation of sound and space. *Proceedings of the National Academy of Sciences*. 2016 Nov; 113(48):E7856-E7865. <http://www.pnas.org/lookup/doi/10.1073/pnas.1612524113>, doi: 10.1073/pnas.1612524113.

1003 Trivedi U, Dieckman E, Xiang N. Reciprocal maximum-length and related sequences in the generation of natural, spatial sounding reverberation. *The Journal of the Acoustical Society of America*. 2009 Apr; 125(4):2735-2735. <http://asa.scitation.org/doi/10.1121/1.4784525>, doi: 10.1121/1.4784525.

1006 Turner RE. Statistical Models for Natural Sounds. PhD Thesis, Gatsby Computational Neuroscience Unit, UCL; 2010.

1008 Watkins PV, Barbour DL. Specialized neuronal adaptation for preserving input sensitivity. *Nature Neuroscience*. 2008 Nov; 11(11):1259-1261. <http://www.nature.com/articles/nn.2201>, doi: 10.1038/nn.2201.

1010 Wen B, Wang GI, Dean I, Delgutte B. Dynamic Range Adaptation to Sound Level Statistics in the Auditory Nerve. *Journal of Neuroscience*. 2009 Nov; 29(44):13797-13808. <https://www.jneurosci.org/lookup/doi/10.1523/JNEUROSCI.5610-08.2009>, doi: 10.1523/JNEUROSCI.5610-08.2009.

1013 Willmore BDB, Schoppe O, King AJ, Schnupp JWH, Harper NS. Incorporating Midbrain Adaptation to Mean Sound Level Improves Models of Auditory Cortical Processing. *Journal of Neuroscience*. 2016 Jan; 36(2):280-289. <http://www.jneurosci.org/cgi/doi/10.1523/JNEUROSCI.2441-15.2016>, doi: 10.1523/JNEUROSCI.2441-15.2016.

1017 Xia J, Xu B, Pentony S, Xu J, Swaminathan J. Effects of reverberation and noise on speech intelligibility in normal-hearing and aided hearing-impaired listeners. *The Journal of the Acoustical Society of America*. 2018 Mar; 143(3):1523-1533. <http://asa.scitation.org/doi/10.1121/1.5026788>, doi: 10.1121/1.5026788.

1020 Yin T. Physiological correlates of the precedence effect and summing localization in the inferior colliculus of the cat. *The Journal of Neuroscience*. 1994 Sep; 14(9):5170-5186. <http://www.jneurosci.org/lookup/doi/10.1523/JNEUROSCI.14-09-05170.1994>, doi: 10.1523/JNEUROSCI.14-09-05170.1994.

1023 Yoshioka T, Sehr A, Delcroix M, Kinoshita K, Maas R, Nakatani T, Kellermann W. Making Machines Understand Us in Reverberant Rooms: Robustness Against Reverberation for Automatic Speech Recognition. *IEEE Signal Processing Magazine*. 2012 Nov; 29(6):114-126. <http://ieeexplore.ieee.org/document/6296524/>, doi: 10.1109/MSP.2012.2205029.

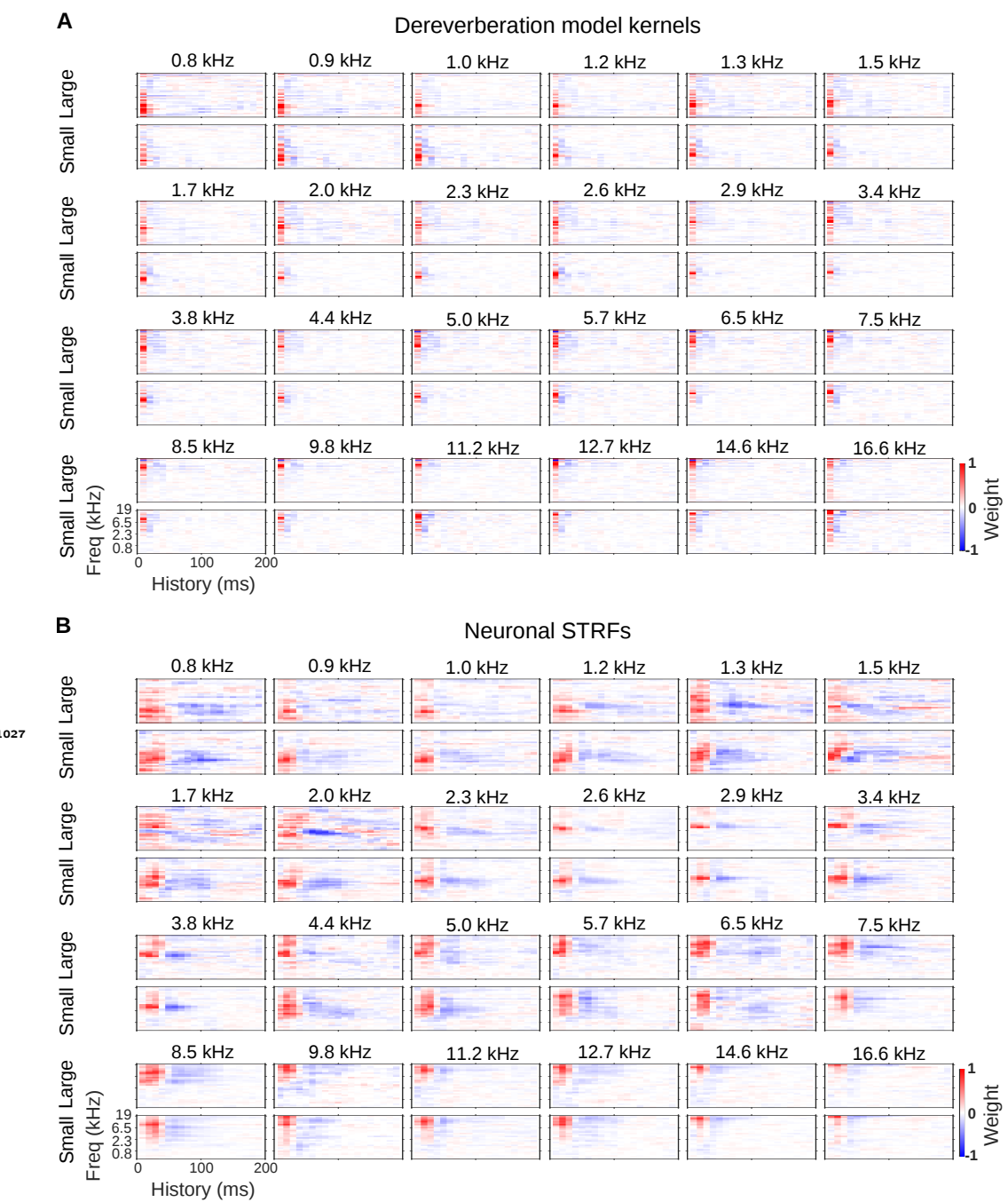


**Figure 2-Figure supplement 1. Model kernels and neuronal STRFs across frequency channels.**

**A**, Model kernels arranged by the anechoic frequency that they were trained to estimate. For each anechoic frequency, the top row shows the kernel for the large room condition, and the bottom row shows the kernel for the small room condition. In each plot, frequency is on the vertical axis and history on the horizontal. **B**, Neuronal STRFs arranged by best frequency, the frequency in the STRF with the largest weight. The STRFs of all neural units with the same best frequency were averaged to produce these plots. Plots are arranged as in A.

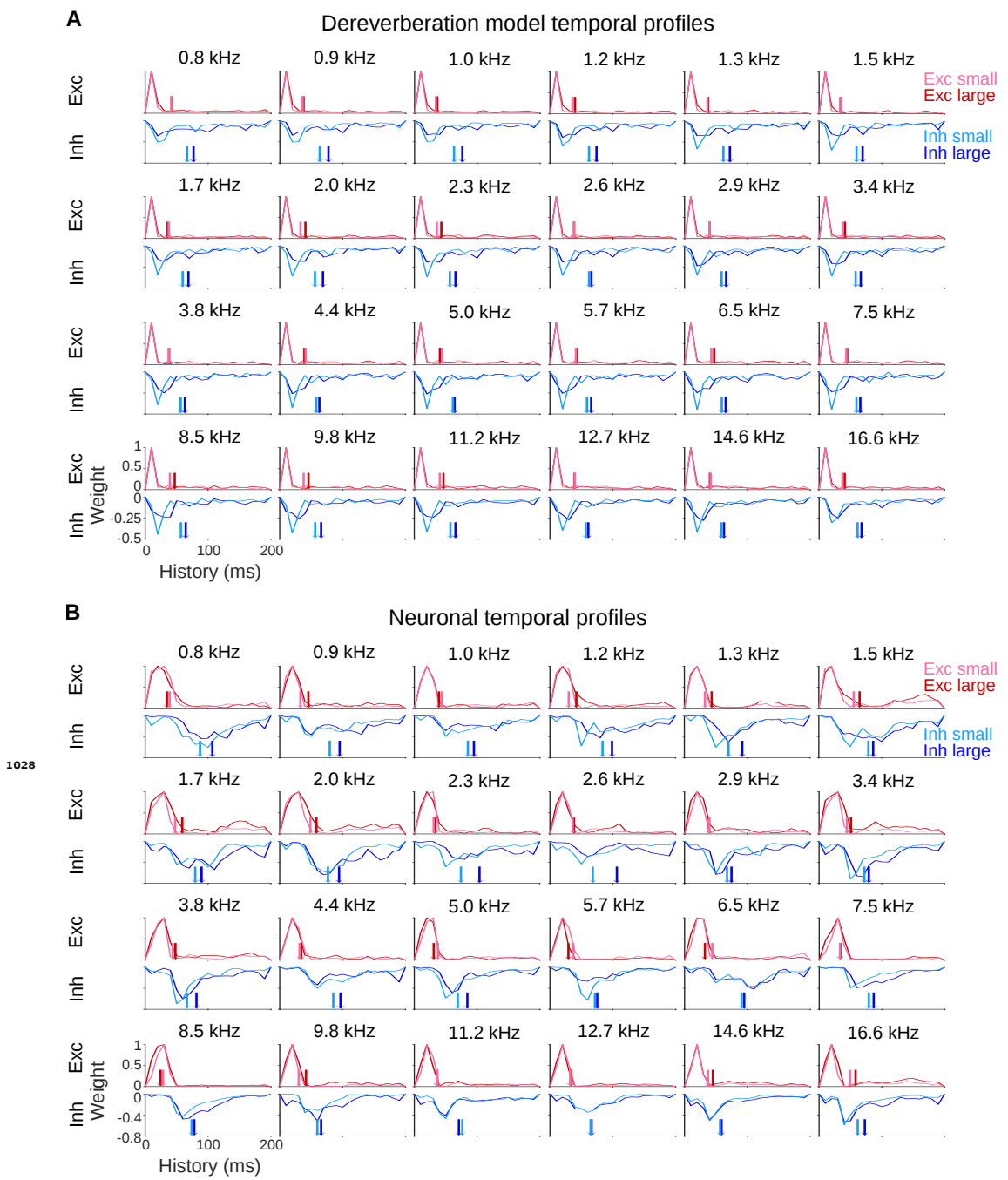


**Figure 2—Figure supplement 2. Model and neuronal temporal profiles across frequency channels.**

**A**, Temporal profiles of the excitatory (top rows) and inhibitory (bottom rows) weights of the model kernels, plotted as in Figure 2B. The estimated anechoic frequency channel is indicated above each pair of plots, as in Figure 2-Figure supplement 1A. The color code is as in Figure 2B: pink = small room excitation; red = large room excitation; cyan = small room inhibition; blue = large room inhibition. The center of mass (*COM*) values for the excitation and the inhibition in each room are indicated by the colored arrows. For each anechoic frequency, each temporal profile was normalized by dividing by the maximum value for the excitatory temporal profile of the same room. **B**, Temporal profiles of the excitatory and inhibitory components of the averaged neuronal STRFs shown in Figure 2-Figure supplement 1B, plotted and normalized as for the model kernels in A.

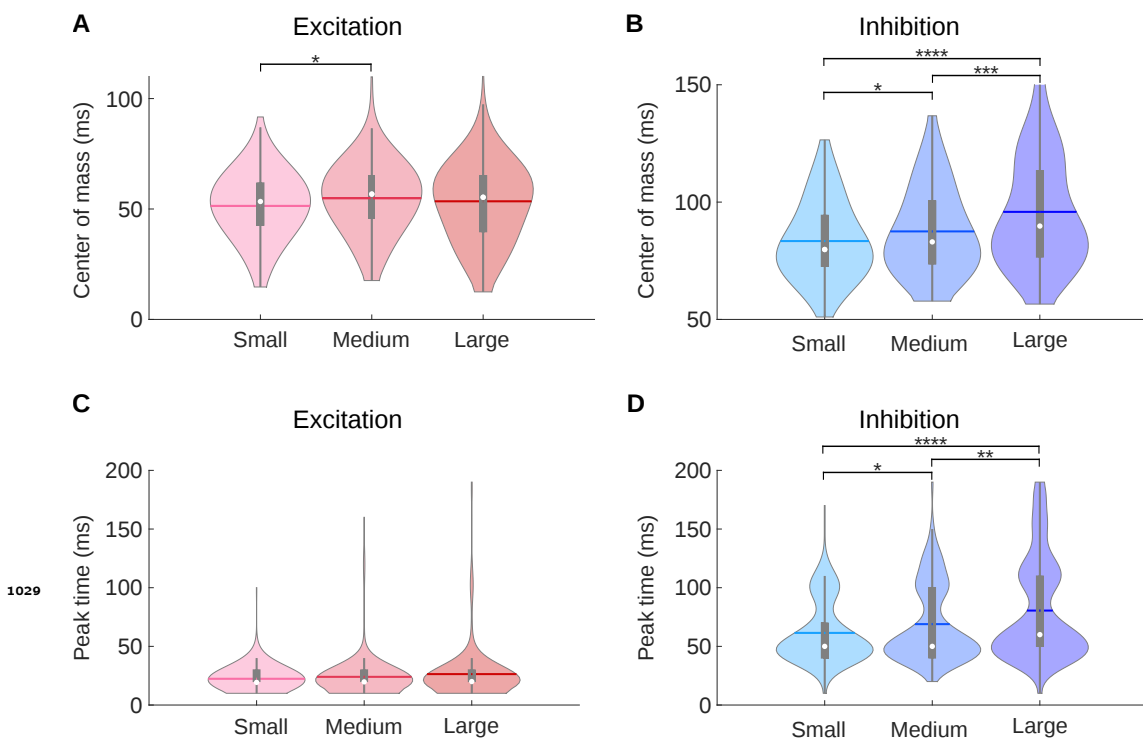


**Figure 3-Figure supplement 1. A medium room condition shows intermediate center of mass and peak time values compared to the small and large room conditions.**

**A**, Violin plots for the center of mass ( $COM^+$ ) of the excitatory fields of the neuronal STRFs for the small, medium and large room conditions computed. **B**, Same as A, but here the violin plots show the center of mass ( $COM^-$ ) of the inhibitory fields for the neuronal STRFs. **C**, Violin plots for the peak time of the excitatory fields ( $PT^+$ ). **D**, The same data as C, but here the violin plots show the peak time ( $PT^-$ ) of the inhibitory fields. In all violin plots, the white dot represents the median, the horizontal thick line the mean, the thick gray lines the interquartile range, the thin gray lines 1.5x interquartile range, and the colored shaded area represents the distribution. The results of Kruskal-Wallis tests followed by multiple comparisons using Fisher's least significant difference (LSD) procedure are indicated above the bars in A, B and D: \*  $p < 0.05$ , \*\*  $p < 0.01$ , \*\*\*  $p < 0.001$ , \*\*\*\*  $p < 0.0001$ .

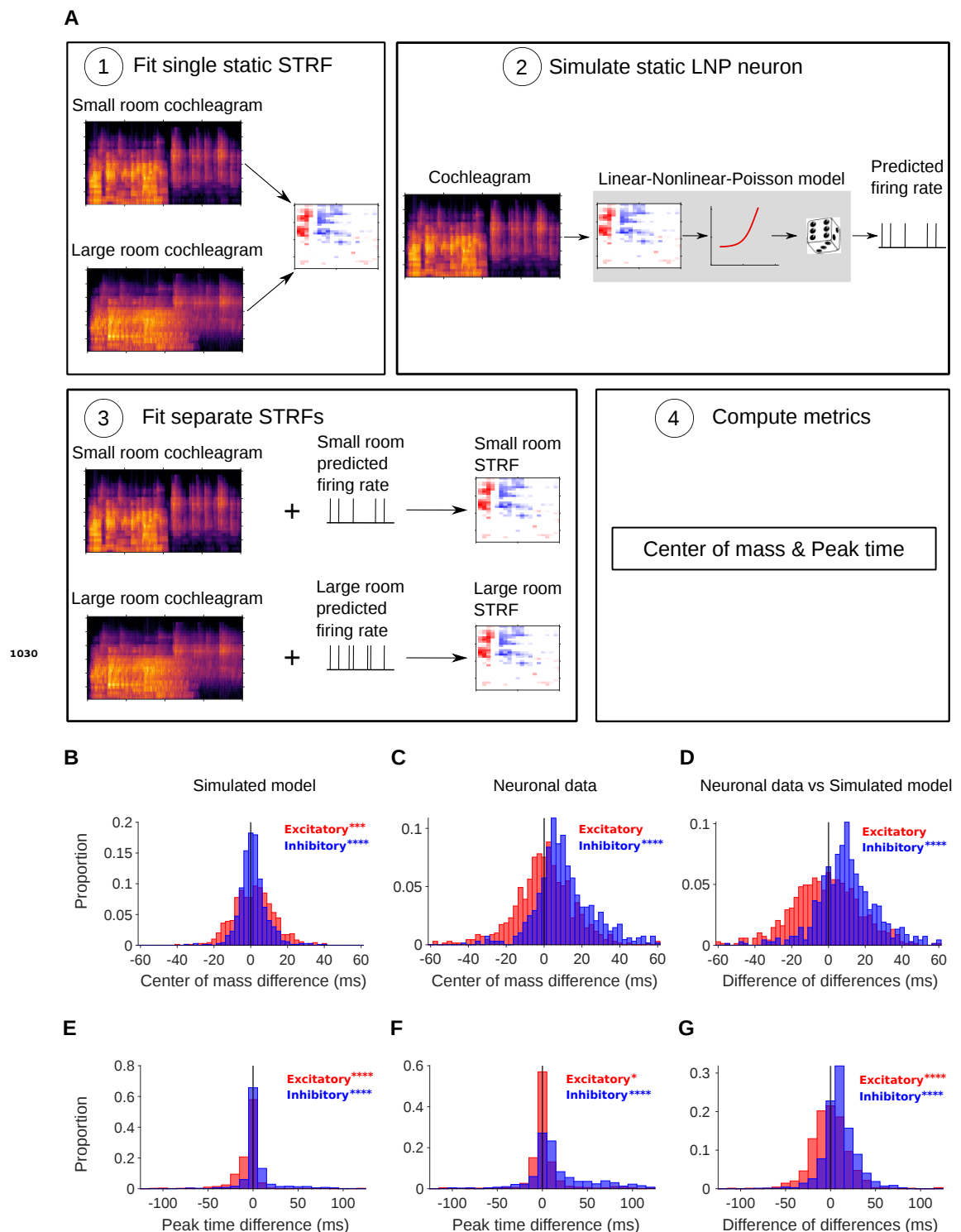


**Figure 3-Figure supplement 2. Simulated neurons suggest a role for adaptation in cortical dereverberation.** See next page for caption.

**Figure 3-Figure supplement 2. Simulated neurons suggest a role for adaptation in cortical dereverberation.**

To confirm that STRF differences between rooms were genuinely a result of adaptation, we simulated the recorded neurons using a non-adaptive linear-nonlinear-Poisson model and compared STRF measures of the simulated responses with those of the real neuronal STRFs in the different room conditions. **A**, The simulated neurons were made in the following way: 1) We fitted a single STRF for each neuron using the combined data from the small and large rooms; 2) We used this STRF along with a fitted non-linearity and a Poisson noise model to generate the simulated firing rate for the small and large rooms separately; 3) Using the small and large room cochleograms and simulated firing rates, we fitted separate STRFs for the two conditions; 4) We computed the center of mass and peak time metrics as before. **B**, Difference in center of mass between the large and small room conditions (large - small room) for the simulated model neurons. The  $COM^-$  values (blue) were slightly larger in the large room, median difference = 0.90ms, and the  $COM^+$  values (red) were slightly elevated too, median difference = 1.7ms. **C**, Reproduction of Figure 3B showing the difference in center of mass of neuronal STRF components between the large and small room conditions (large - small room). The  $COM^-$  values increased in the larger room (median difference = 9.3ms), whereas  $COM^+$  did not differ significantly (median difference = 0.32ms). **D**, The center of mass differences shown in B and C were subtracted for each unit and plotted as the resulting difference of differences (real cortical unit - simulated model neuron). The  $COM^-$  differences between rooms were consistently larger in the neuronal data (median difference = 9.3ms), while the  $COM^+$  differences did not differ significantly (median difference = -1.1ms). **E**, Difference in peak time between the large and small rooms (large - small) for the simulated model neurons. The  $PT^-$  median difference = 0ms and the  $PT^+$  median difference = 0ms. **F**, Reproduction of Figure 3D showing the difference in peak time between the large and small rooms (large - small), calculated from neuronal STRFs. The  $PT^-$  values were larger in the large room (median difference = 10ms).  $PT^+$  did differ significantly between the rooms, but with a median difference = 0ms. **G**, Histogram of the difference in peak time room differences between the neural units and corresponding simulated model neurons (neural unit - simulated model neuron), plotted as in D above. The  $PT^-$  values were consistently larger in the large room for the neuronal data vs the simulated model neurons (median difference = 10ms).  $PT^+$  did significantly differ, but the median difference = 0ms. Asterisks indicate the significance of Wilcoxon signed-rank tests: \*\*\*\* $p < 0.0001$ , \*\*\* $p < 0.001$ , \* $p < 0.05$ .

1031

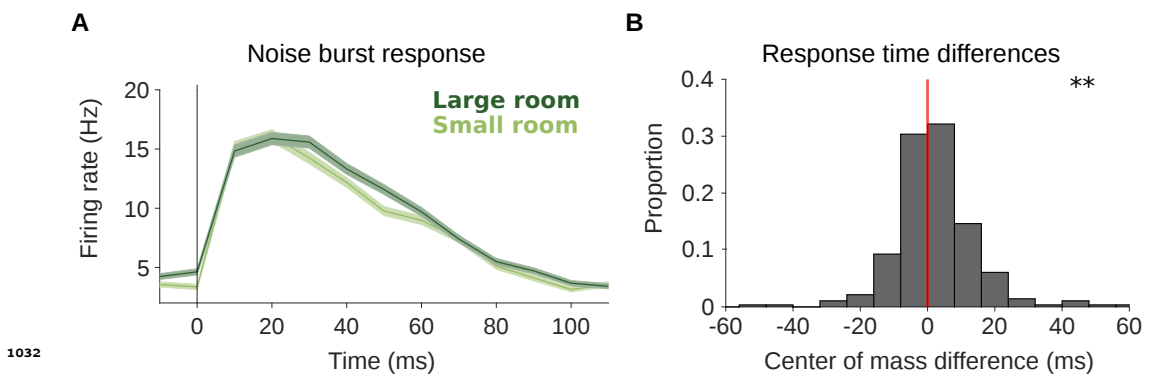


**Figure 3-Figure supplement 3. Neural response to noise probe shows slower adaptation in the more reverberant condition.**

**A**, Average firing rate across all cortical units in response to a noise burst that was embedded within the reverberant stimuli. Responses to the noise within the small (light green) and large (dark green) rooms are plotted separately. Shaded areas show  $\pm$ SEM across units. The vertical line indicates the noise onset. **B**, Histogram of the difference in center of mass of the neuronal response to the noise probe (shown in A) between the two room conditions (large - small room). The center of mass shifted to a later time in the larger room (median difference = 1.0ms). Asterisks indicate significance of a Wilcoxon signed-rank test: \*\* $p < 0.01$ .

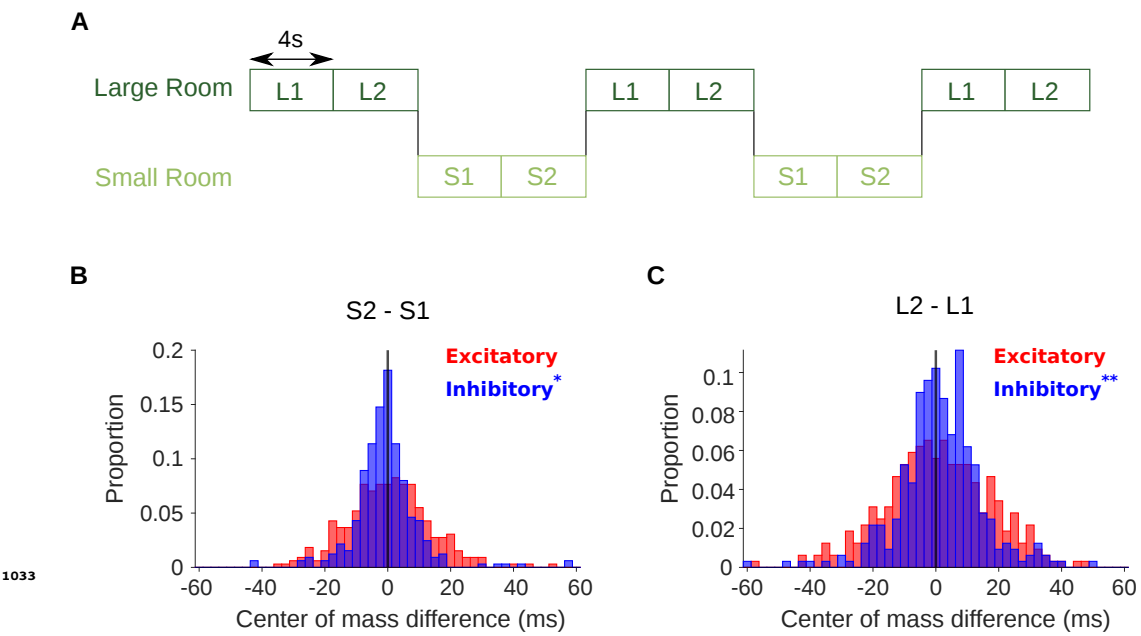


**Figure 3-Figure supplement 4. Adaptation to reverberation is confirmed using stimuli that switch between the small and large room.**

**A**, Schematic shows the structure of the stimulus, which switched between the large (dark green) and small room (light green) conditions. Letters indicate the reverberant condition in each stimulus block (S: small room, L: large room). Each 8s block within a given room condition was divided for analysis into an early (S1,L1) and late (S2,L2) period. STRFs were fitted to the data from each of the 4 periods independently (S1, S2, L1, L2). **B**, Difference in center of mass of inhibitory ( $COM^-$ , blue) and excitatory ( $COM^+$ , red) STRF components between the late and early time period of the small room stimuli (S2 - S1, see A). The  $COM^-$  decreased in S2 relative to S1 with a median difference = -0.9ms;  $COM^+$  did not differ significantly, median difference = 0.52ms. **C**, Center of mass difference plotted as in B, but for the large room stimuli (L2 - L1). The  $COM^-$  values were larger in L2 relative to L1, median difference = 1.5ms, while the  $COM^+$  values were not significantly different, median difference = 0.8ms. Asterisks indicate the significance of Wilcoxon signed-rank tests: \*\* $p < 0.01$ , \* $p < 0.05$ .